NOVA SCHOOL OF SCIENCE & TECHNOLOGY

DEPARTAMENT OF MATERIALS SCIENCE

TOMÁS FRANCISCO PRIOR VICENTE DE MEDEIROS PEREIRA

BSc in Micro and Nanotechnology Engineering

PRINTED TRANSPARENT CONDUCTIVE OXIDES FOR ELECTRONIC APPLICATIONS

MASTERS IN MICRO AND NANO TECHNOLOGY ENGINEERING

NOVA School of Science and Technology

03, 2023

NOVA SCHOOL OF SCIENCE & TECHNOLOGY

DEPARTMENT OF MATERIAL SCIENCES

PRINTED TRANSPARENT CONDUCTIVE OXIDES FOR ELECTRONIC APPLICATIONS

TOMÁS FRANCISCO PRIOR VICENTE DE MEDEIROS PEREIRA
BSc in Micro and Nanotechnology Engineering

Adviser: Rita Mourão Salazar Branquinho,
Invited Assistant Professor, NOVA School of Science and Technology

Co-Adviser: Emanuel Abreu Antunes Gameiro Carlos,
Assistant Researcher, NOVA School of Science and Technology

Examination Comitee:

Chair: Rui Alberto Garção Barreira do Nascimento Igreja,
Associate Professor, NOVA University Lisbon

Rapporteurs: Pedro Miguel Cândido Barquinha,
Associate Professor, NOVA University Lisbon

Adviser: Rita Mourão Salazar Branquinho,
Invited Assistant Professor, NOVA University Lisbon

MASTER IN MICRO AND NANOTECHNOLOGY ENGINEERING

NOVA School of Science and Technology
03, 2023

AGRADECIMENTOS

Encontro-me na feliz posição de ter bastante a agradecer.

Primeiramente à Faculdade de Ciências e Tecnologias da Universidade Nova de Lisboa, pelas condições que me vem oferecendo nos últimos 5 anos. Em particular, sobretudo no âmbito deste trabalho, mas não só, ao Departamento de Ciências dos Materiais bem como ao CENIMAT|I3N e CEMOP por todas as condições que foram proporcionando ao longo do meu percurso académico que culmina com neste trabalho. Also, I acknowledge the European Community's H2020 program [Grant Agreement No. 101008701 (EMERGE, H2020-INFRAIA-2020-1) and No. 951774 (FOXES, H2020-EIC-FETPROACT-2019)] and project IDS-Paper PTDC/CTM-PAM/4241/2020 from FCT-MCTES.

Um enorme obrigado aos meus orientadores, Rita Branquinho e Emanuel Carlos por estarem sempre disponíveis para me receber. Desde o primeiro dia estiveram presentes, mesmo quando não tinham de o estar, sempre disponíveis para aconselhar e ouvir. Nenhuma dúvida ficou por esclarecer e é graças a vocês que concluo o meu percurso e não poderia estar mais contente. Não me imagino a percorrer os caminhos sinuosos do mestrado com outra orientação.

Uma nota de valor aos meus monitores, Raquel Martins e Pedro Moreira por terem tido a paciência e compreensão de me acompanharem, vezes sem conta, pelos laboratórios e sempre com uma enorme boa disposição. Agradecer aos demais companheiros de laboratório e sobretudo à Alexandra Gonçalves e Marta Luís por terem sido como que um farol sempre que estava perdido ou precisava de algo. Para além do apoio imprescindível, foram uma presença com um constante sorriso e sentido de humor para aliviar as minhas ocasionais neuras.

Agora para os meus amigos, por ordem de antiguidade do grupo. Começar pela malta da escolinha, Ricardo, Vasco, Calado, Lua e David, é de boca cheia que vos chamo meus amigos, todos incríveis e com um papel importante na minha vida, se não tivessem feito parte da minha caminhada por certo seria uma pessoa diferente. Uma nota especial para o Ricardo por nestes últimos anos ter assumido o papel de confidente que agora vai ter de arcar para o resto da vida, azarinho. Para o Edu, Fialho e Ruben, obrigado pela diversão, por me ensinarem a relaxar e a confiar nos outros, pelos risos e brincadeiras que prezo e pela paciência que tiveram em todos os momentos, bons e maus. Aviso já que não vou permitir afastamentos. Por fim, a malta da faculdade, os com quem tive o prazer de partilhar o curso de MIEMN, Michele, Sousa, Mariana, Cristo, pela motivação e acompanhamento que me têm dado, sem a vossa presença não teria acabado o mestrado, isso ou teria acabado mais cedo, perguntas que nunca terão resposta. Convosco é sempre assim, mas não quereria de outra forma, prezo os momentos que partilhámos e sei que vamos continuar a partilhar. Ainda no curso, um agradecimento à Mariana Abreu pela motivação que vai dando, à maneira dela e, que foi funcionando de quando em vez, e a todos os restantes pela solidariedade e união com que me presentearam nos últimos 5 anos,

não serão esquecidos. Tenho ainda a nomear, pessoas que foram entrando avulsamente e que merecem a presença, à Maria, Joana, Cátia e Riccardo, obrigado por terem participado neste capítulo, que assim se mantenha.

Por último, à minha família, a começar pelos meus pais por tudo o que tiveram de passar e por não terem baixado os braços. Um agradecimento muito especial à minha avó por ser das pessoas mais sábias que passaram na minha vida, espero que continuemos com as nossas conversas e a darmos alegrias um ao outro. A toda a minha restante família, obrigado pela preocupação e carinho que foram demonstrando, apesar da distância é sempre encorajador saber que não estamos esquecidos.

“You cannot teach a man anything; you can only help him discover it in himself.”
(Galileo)

Abstract

Transparent conducting oxides (TCOs) are nowadays a large market with various important applications specially in the field of optoelectronics, such as LCDs, touch screens, solar panels, among others. Despite the recent advancements, the main processes to produce such materials still employ highly expensive methods based on vacuum environment. This work focusses on the production of In_2O_3 (the most commonly used material, presenting great optical properties and, after doping, great electrical properties) thin films via solution combustion synthesis (SCS), a low-cost alternative, and is divided in two steps. The first step focussed on producing, via spin coating, the most adequate thin film by changing the indium concentration the number of layers, the solvent, to decrease the environmental impact, and the ethylene glycol (EG) concentration, to control the physical properties in preparation for the second step. All thin films were doped with Zr, a type-III donor, being the most promising thin film based on ethanol, a green solvent, with a 20% (EG) concentration (V/V) an In_2O_3 concentration of 0.2M and 8 layers, that presented high transparency in the visible range (350 nm to 750 nm) of 82.99%, and a bulk resistivity of 2.82×10^{-1} Ω.cm. Focusing exclusively on electrical performance, the most promising film was a 2-methoxyethanol based film, without EG, for an In_2O_3 concentration of 0.2M and 8 layers presented a transparency in the visible range of 83.85% and a bulk resistivity of 9.34×10^{-2} Ω.cm. Once found the most promising thin film conditions (ink viscosity, electrical properties, and environmental impact) the solution based on ethanol was implemented on inkjet printing ensuring a proper deposition. For this phase, UV pre-treatment of the substrate, Z-value, printing resolution (number of dpi) and number of layers parameters were tested. The main property to be analysed in this work is the film uniformity, with promising results being achieved with uniform films being obtained with a UV pre-treatment on the substrate for 15 minutes, a resolution between 400 DPIs and 800 DPIs and a single layer.

Keywords: Transparent conducting oxide, solution combustion synthesis, green solvents, zirconium-doped indium oxide thin films, Inkjet printing.

Resumo

Óxidos condutores transparentes (TCOs) representam atualmente um mercado enorme com várias aplicações importantes, especialmente no ramo da optoelectrónica, tais como LCDs, ecrãs táteis, painéis solares, entre outros. Apesar de avanços recentes, os principais processos de produção destes materiais ainda dependem de métodos bastante dispendiosos baseados em técnicas de alto vácuo. O foco deste trabalho passa pela produção de filmes finos de In_2O_3 (o material mais utilizado, por apresentar boas propriedades óticas e, depois de dopado, boas propriedades elétricas) por síntese de combustão em solução (SCS), uma alternativa mais económica, e está dividido em dois passos. O primeiro passo é a produção, por *spin coating*, do filme fino mais adequado variando a concentração de índio, o número de camadas, o solvente minimizando o impacto ambiental e a concentração de etilenoglicol (EG) de modo a controlar as propriedades físicas em preparação para o segundo passo. Todos os filmes finos foram dopados com Zr tendo sido o mais promissor aquele cujo solvente era o etanol, um solvente sustentável, com uma concentração de EG de 20% (V/V) uma concentração de In_2O_3 de 0.2M e 8 camadas, que apresentou um filme com uma transparência na zona do visível (350nm a 750nm) de 82.99% e uma resistividade em volume de 2.82×10^{-1} Ω.cm. Com foco exclusivamente no desempenho elétrico, o filme mais promissor tinha como solvente 2-metoxietanol, sem EG, com uma concentração de In_2O_3 de 0.2M e 8 camadas, apresentava uma transparência na região visível do espetro de 83.85% e uma resistividade em volume de 9.34×10^{-2} Ω.cm. Uma vez encontrado o filme fino com as condições mais promissoras (viscosidade da tinta, propriedades elétricas e impacto ambiental), a solução baseada em etanol foi implementada por impressão a jato de tinta garantido uma deposição adequada. Nesta fase, o pré-tratamento por UV do substrato, *Z-value*, resolução da deposição (número de DPIs) e número de camadas foram testados. A propriedade analisada foi a uniformidade do filme, apresentando resultados promissores usando um pré-tratamento UV por 15 minutos do substrato, uma resolução entre os 400 e os 800 DPI e uma única camada.

Palavras-chave: Óxidos condutores transparentes, síntese de solução por combustão, solventes sustentáveis, filmes finos de óxido de índio dopado com zircónio, *inkjet printing*.

Contents

List Of Figures

List Of Tables

Acronyms

2-ME	2-Methoxyethanol
ATR	Attenuated Total Reflectance
CAGR	Compound Annual Growth Rate
CB	Conduction Band
CBM	Conduction Band Minimum
CIJ	Continuous Inkjet
DPIs	Dots per Inch
d_s	Film Thickness
DOD	Drop on Demand
DSC	Differential Scanning calorimetry
EG	Ethylene Glycol
ETH	Ethanol
FTIR	Fourier Transformed Infrared Spectroscopy
IPA	Isopropyl Alcohol
ITO	Indium Tin Oxide
LAFPD	Large Area Flat Panel Display

NIR	Near Infrared
PTFE	Hydrophobic Polytetrafluoroethylene
SCS	Solution Combustion Synthesis
SDS	Sodium Lauryl Sulphate
TCO	Transparent conducting Oxide
TCM	Transparent conducting material
TFSC	Thin Film Solar Cell
TG	Thermogravimetry
TM	Transition Metal
TSE	Touch Screen Electrode
UV	Ultraviolet
Vis	Visible
z	Distance to substrate

Symbols

d	Nozzle size
E_f	Fermi level
E_g	Energy bandgap
E_{opt}	Optical bandgap
h	Planck's constant
M	Molar concentration
m^*	Electron effective mass
n	Carrier concentration
α	Absorption coefficient
γ	Surface tension
η	Dynamic viscosity
μ	Carrier mobility
ν	Frequency
ρ	Density
σ	Conductivity

Motivation and Objectives

Nowadays, transparent conducting oxides (TCOs) play a crucial role in the transparent electronics research field, with growth tendency estimates from 8% to 10% GAGR.[1]–[3].

A lot of common use devices, such as smartphones, wearables, solar panels, to name a few, all require TCOs for their functioning. Which would explain the increase in demand for these materials, as the devices themselves become more widespread.

However, yet, many of the processes employed require high vacuum and noble gases, increasing their cost, therefore limiting their viability. With this in mind, the development of manufacturing alternatives is of the highest importance. Solution based processes, such as solution combustion synthesis, as opposed to the more common production methods, don't require neither vacuum nor noble gases. Furthermore, the employment of these methods allows for deposition by inkjet, for example, which is an additive method, disregarding the need of masks and etching, allowing further reduction of the cost when compared to conventional methods. These processes can use a plethora of different solvents and precursors, this work, based on a previous work, has an approach more focused on sustainability, employing more sustainable solvents through. And hopes to lay the ground for inkjet printing implementation.

The main objectives of this work are:

- Optimize the In_2O_3 solution combustion synthesis parameters for both spin coating and inkjet printing of TCO thin films.
- Produce solution based In_2O_3 TCO thin films via spin coating and characterize them.
- Implement an eco-friendlier solvent alternative to produce TCO thin films and characterize them.
- Implement the most promising solution based In_2O_3 ink via inkjet printing and optimize the printing conditions, in order to obtain even TCO thin films.

1. INTRODUCTION

1.1. Transparent conducting oxides (TCOs)

Transparent conducting oxides (TCOs) are transparent conducting materials (TCMs) that, as the name suggests, present both electrical conductivity and transparency in the visible range of the spectrum, which requires a bandgap above 3 eV [4], [5]. However, usually this combination of properties is not very common, most transparent materials are insulators and the electrically conductive materials do not present the desired transparency[6].

Nowadays, Transparent Conducting Material (TCMs) are fundamental materials for various commercial applications, some of which are depicted in Figure 1.1. [7]–[10]

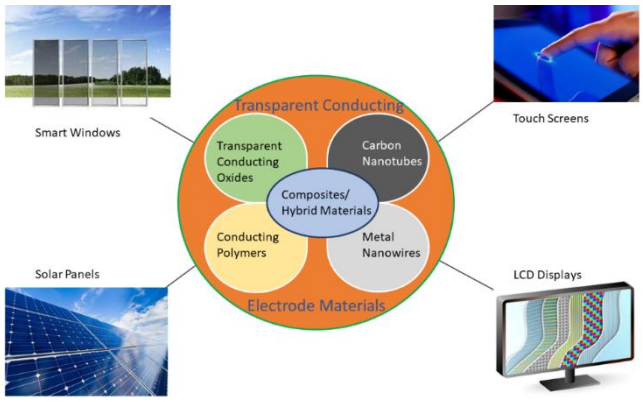

Figure 1.1- Main TCM applications

Images adapted from [17-20]

Despite this materials rarity, the first TCO was introduced over a century ago, by K. Bädeker, in 1909[11]. Using thermal oxidation of a thin metal film of cadmium (Cd) deposited by sputtering they obtained Cadmium Oxide (CdO), the first TCO. However, CdO's thin film toxicity and narrow band gap limited its applications, even though, through doping, it presented very appealing results, such as a low resistivity and high transmittance[12], [13].

Later, in the 1960s, indium tin oxide (ITO) was introduced and is still the main TCO material employed up to this day in electronic devices, and is expected to remain in this position for at least a

few more years[14]–[16]. However, the high vacuum fabrication method employed, sputtering, increases its cost, calling for alternative processes[14], [17]–[20].

When approaching TCOs it is important to be aware of the main parameters to take into consideration. Given the applications, it needs to present both good electrical and optical properties. The main electrical property is the conductivity, which is given by: $\sigma=\mu \cdot n \cdot e$, where μ is the electron mobility, n is its carrier concentration and e is the electron charge, with the mobility (μ) being given by[4], [5]:

$$\mu = \frac{e\tau}{m^*} \tag{1.1}$$

Where τ is the average scattering time and m^* is the effective electron mass. On the other hand, the main optical properties to consider are the optical bandgap which, in order to achieve transparency, must be higher than 3 eV and show a low absorption coefficient in the UV-VIS-NIR region. The fraction of the flux absorbed in a film (A), combines the optical and electrical properties of a film is given by[5]:

$$A \cong 1 - e^{(\frac{\alpha}{\sigma R})} \tag{1.2}$$

Where α is the absorption coefficient, σ electrical conductivity and R the reflectance. Both these properties must be considered simultaneously. Since TCOs are semiconductors, their conductivity depends, among other factors, on the doping, both on the dopant itself and the doping percentage, which in turn influences the optical properties. Also, the thickness of the film and its uniformity are relevant parameters that affect both properties[5].

1.2. **Indium Oxide Doping**

Since TCOs are semiconductors by nature, their conductive properties are highly reliant on doping agents, each resulting in different effects on the final product.

One way to create free carriers is through intrinsic doping, achieved by film stoichiometry variation. Moreover, altering the growth conditions results in changes to the film, and oxygen deficient conditions result in a larger amount of defects which is the case for vacuum or a reducing atmosphere post processing as well. [21], [22]

Though, extrinsic doping, gives a better control over the optical and electrical properties, as well as better stability when compared to intrinsic doping which is the most popular approach.

One common strategy has been using transition metals (TM) as dopants for n-type TCOs, such as tin indium (ITO). Depending on their d-orbital levels position relative to the conduction band minimum and to the Fermi level (E_F), TMs can be classified into three categories: type-I, II or III. The usual approach is to employ as dopant a same period next row element to avoid disturbing the crystalline structure[23]. Sn has been commonly used as a dopant for ITO, however, it may reduce the intrinsic carrier mobility (μ) due to an increase in the electron effective mass (m^*). Besides, Sn dopant can only donate one electron to In_2O_3, requiring a high density of dopant to achieve the desired carrier density (n_e)[24], calling for a replacement.

To achieve the best mobility and donate sufficient electrons into the conduction band (CB) of the In_2O_3, the dopant should have its donor level high inside the conduction band, as shown in Figure 1.2.

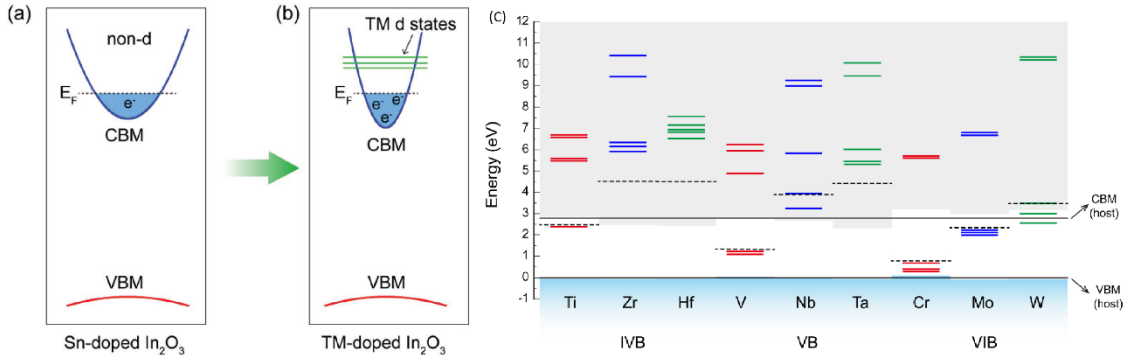

Figure 1.2-Schematic diagram of the band structures for a) Sn-doped and b) ideal TM-doped In_2O_3 and c) Different type dopants [15].

Based on the analysis of Figure 1.2 c), it is possible to assess that, type-I dopants (Ti, V and Cr) are not the most suitable for conduction as their *d* orbital energy levels are below the conduction band minimum (CBM). Type-II dopants (Nb, Mo and W) despite having higher *d* orbital energy levels than the same group are lower period dopants which still shows inadequate doping. Given the proximity of E_F to the *d* orbital energy level, this will contribute to an increase in m^* not allowing optimal electrical performance. However, Type-III dopants (Zr, Hf and Ta) present a *d* orbital energy level well above both the CBM and E_F, presenting the highest potential to be used as dopants in indium oxide.

1.3. Solution Combustion Synthesis (SCS)

Solution combustion synthesis (SCS) is a chemical production method for oxide materials, that derives from sol-gel synthesis[25]. The major advantage of solution-based synthesis processes when compared to vacuum-based processes is their efficiency and cost. The energy costs and material waste are greatly reduced. This type of synthesis allows for multiple deposition methods such as spin coating[18], [26], inkjet printing[27], [28], dip coating[29], flexographic printing[30], amongst others[4], [31].

Comparing SCS directly with other solution synthesis methods, such as the conventional sol-gel, this method requires a lower temperature to form the metal oxides. Whereas conventional sol-gel, relies solely on external heating, SCS employs a fuel that provides further energy to the formation of the oxide via an exothermic reaction rather than just depending on external heating. This means, in SCS, after an initial energy is provided (electrical or thermal), upon reaching the ignition temperature (T_{ig}), a self-sustained redox reaction between the precursor (like metal nitrates) and the fuel occurs, this results in liberation of heat by formation of CO_2 and H_2O. This means that, the external heating applied can be lowered, allowing for deposition on a broader range of substrates, particularly sensitive substrates such as transparent flexible polymers.

The SCS main steps are shown in Figure 1.3. Firstly, the precursor solution is prepared, it combines a solvent, with a metal precursor and an organic fuel. For solvents, water is the most common one, but other organic solvents like ethanol (ETH) or 2-methoxyethanol (2-ME) have been used when water isn't suitable. For the metal precursors, considering the counter anion role in the combustion

synthesis, they can be classified as, oxidants, reducers, or neutrals. The oxidants are metal nitrates or nitrate hydrates, such as indium (III) nitrate hydrate, these present great oxidizing power, solubility in water and polar solvents and low decomposition temperatures. Other metal precursors, such as oxalates, alkoxides, acetates and acetylacetonates act as reducers, these however, require additional oxidants. As for neutral precursors, these are chlorine-based that can contaminate the resulting film and, as a by-product, release HCl[32], [33]. When it comes to the fuel to be used in a solution, it is important to note all the demands that an ideal fuel must fulfil concerning the final product. Firstly, it acts as the reducer of the reaction and should be able to, at a lower temperature, undergo combustion. Furthermore, it behaves as a chelating agent that enforces a proper structure and homogeneity of the final product. There are several types of fuels, even several ways to classify them, being the most relevant the functional group they present. Urea (CH_4N_2O) is the most used fuel, it presents two amino functional groups, as opposed to fuels presenting carboxylic groups (-COOH) like ascorbic acid ($C_6H_8O_6$) or hydroxyl groups (-OH) like ethylene glycol. They mainly differ on the intensity of the redox reduction, where amino groups are the most redox active[33]. Another advantage, besides the oxidating power, of urea is its abundance and enhanced coordination ability relative to metal nitrate precursors.

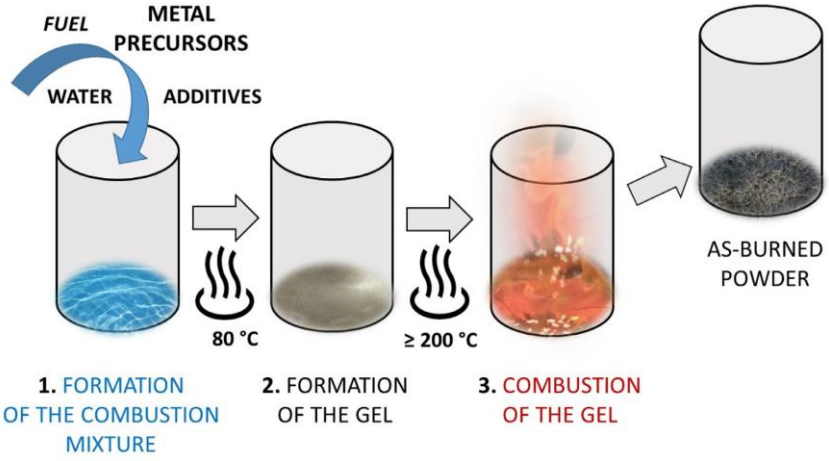

Figure 1.3-Schematic of the main steps of SCS [22]

For indium oxide (In_2O_3) formation, it can be represented by the following equation:

$$2In(NO_3)_3 \cdot 2H_2O + CO(NH_2)_2 \rightarrow In_2O_3 + 4H_2O + CO_2 + 4N_2 + 6O_2 \quad (1.3)$$

The first thin film based on this method was developed in 2003 by *Epifani* et al. where acetylacetone was used as a chelating agent and fuel to create an ITO thin film [32]. Ever since, multiple TCOs have been developed using this technique, presenting various property differences based on the different precursors, deposition techniques, temperatures, and fuels.

Table 1.1 summarizes some of the developments over the last decade, resorting to spin coating deposition. Based on this table, it is possible to verify the range of control solution synthesis provides, allowing for temperature ranges from 160 °C to 600 °C depending on the materials and annealing/curing conditions. Moreover, SCS can be combined with ultraviolet (UV) irradiation, allowing an improvement in the quality of the films, whilst further reducing the processing temperature.

When SCS is employed in conjunction with UV irradiation, the UV irradiation has high-energy photons that facilitate the M-O-M network formation by activating the metal and oxygen atoms. Further irradiation contributes to complete condensation and film densification by rapidly decreasing the oxygen and carbon contents[32]. This effect contributes to better performing films at lower temperatures.

Table 1.1- Properties of different TCO electrodes for different deposition methods and different materials and deposition temperatures (note, * stands for UV exposed film post annealing).

Year	TCO	Dopant	Annealing temperature (°C)	Deposition Method	Bulk resistivity ($\times 10^{-1}$ Ω.cm)
2012 [14]	In_2O_3	Sn (10 cat%)	300	Spin-Coating	0.0459
2017 [34]	In_2O_3	Sn (10 wt%)	300	Sputtering	0.0025
2018 [35]	In_2O_3	Ce (3.7%)	500	Spin-Coating	0.0129
2018 [35]	In_2O_3	Sn (1.36%)	500	Spin-Coating	0.0242
2018 [36]	In_2O_3	Ti (0.3M)	450	Spin-Coating	0.5000
2020 [37]	In_2O_3	W (0.5 at%)	500	Spin-Coating	0.0054
2021 [38]	In_2O_3	Hf (0.5%M)	600	Spin-Coating	0.0400
2021 [39]	In_2O_3	Zr (1%M)	400	Spin-Coating	0.0730
2022 [40]	ZnO	-	160*	Spin-Coating	0.0217

1.4. **Printed TCOs**

Despite the practicality and popularity of spin-coating as a deposition method for TCO thin-film, there are alternatives presenting higher throughput and less material waste such as inkjet printing[27], [41]. Inkjet printing is an additive, maskless, non-contact simple and fast process, that doesn't require etching and is compatible with multiple substrates, all these properties contribute for a low cost deposition[41], [42]. It can be divided into two types, continuous inkjet (CIJ), where there is a constant flow of ink, and the individual droplets are selectively charged and either get deflected by electric charge on the deflection electrode or are recycled back into the ink tank. Drop on demand inkjet (DOD) is the other type, where individual droplets are released directly onto the substrate as required.[43] Within DOD, there are multiples ways to control the selective release of droplets. There is a thermal process, where a thin film resistive heater on the nozzle vaporizes the ink to form small bubbles, for this to work, the ink must be vaporizable, another challenge this method might face is the deposition on more sensitive substrates, due to the heating. A more versatile alternative is the piezoelectric method where a piezoelectric transducer generates, by application of an electric signal, a mechanical pulse that increases the pressure in the nozzle releasing the droplets[43], [44]. DOD, besides presenting less material waste when compared to CIJ, also presents a higher resolution, drops diameter vary from 20-30 µm as opposed to 100 µm of the CIJ[42], [44]. Inkjet printing relies on several ink properties for adequate deposition, these include, the viscosity, surface tension, density, used to determine the Z-value, that should be between 1 and 10[41], [44].

2.

Materials and Methods

This section explains the main procedures and techniques used during this work, concerning the production of the zirconium doped indium oxide thin films, as well as their electrical characterisation. Different parameters such as the solvent (water, ethanol, and 2-ME), the indium concentration, and the number of layers were studied to define the best condition to apply for TCOs production. The best performing condition by spin-coating considering the previous parameters was implemented in inkjet printing where the printing conditions were optimized (DPIs, pre-treatment, among others).

2.1. Indium Precursor solution preparation and characterization

The metallic oxide precursor solutions were prepared by dissolving indium (III) nitrate hydrate ($In(NO_3)_3 \cdot xH_2O$, Sigma, 99.9%, CAS 207398-97-8), in 2-methoxyethanol (2-ME, $CH_3OCH_2CH_2OH$, Alfa Aesar, 99%, CAS 109-86-4) with a molar concentration of 0.1 M and 0.2 M. This was followed by adding zirconium (IV) oxynitrate hydrate ($ZrO(NO_3)_2 \cdot xH_2O$, Sigma, 99%, CAS 14985-18-3) in 1%M proportion. Zr was chosen as the dopant based on the properties presented previously and the doping concentration was determined in a previous work, based on the lowest bulk resistivity.[39] Then the fuel, urea ($CO(NH_2)_2$, Sigma, CAS 57-13-6) was added with a molar ratio between urea and indium nitrate of 2.5:1 to ensure the redox stoichiometry of the reaction. Lastly ethylene glycol (EG, CH_2OHCH_2OH, Carlo Erba, CAS 107-21-1) was added in concentrations ranging from 0%(V/V) to 15%(V/V).

For the second stage, the metallic oxide precursor solutions were prepared by dissolving indium (III) nitrate in ethanol absolute (ETH, CH_3CH_2OH, PanReac AppliChem, CAS 64-17-5) or ultrapure water, followed by zirconium (IV) oxynitrate hydrate in a 1%M proportion. Then, the ethylene glycol was added in concentrations ranging from 10%(V/V) to 25%(V/V) to the previous solvents. In the water solution, due to hydrophobic behaviour when deposited on the substrate, a surfactant was added to promote the adhesion, sodium lauryl sulfate (SDS, $C_{12}H_{25}NaO_4S$, Scharlau, 95%, CAS 151-21-3).

All the solutions were stirred at 450 rpm for, at least, 1 hour and a half at 25°C before use.

Next, the solutions and the precursors and solvents (annex A) were chemically analysed by Fourier Transform Infrared Spectroscopy (FTIR), using an Attenuated Total Reflectance (ATR) sampling accessory (Smart iTR) equipped with a single bounce diamond crystal on a Thermo Nicolet 6700 spectrometer. The spectra were acquired in the range of 4500-525 cm^{-1}. The viscosity of the solutions was determined by a CAP 2000+ Viscometer, from Brookfield, using a Cap09 Spindle and a volume of 67

µL per sample. Each condition was measured using 2 samples and each sample measured thrice. The measurements employed a hold of 30 seconds and a run time of 30 seconds, for the 2-ME solutions 400 rpm were used at 25◦C whereas ETH samples required 500 rpm for an accurate measurement. Later, based on the viscosity values obtained the Z-value was determined (the calculation is explained in annex B).

2.2. Thin film deposition and characterization

Both silicon wafer and Corning eagle glass, with a size of 2.5 × 2.5 cm^2, underwent a cleaning process consisting in an ultrasonic bath for 10 minutes in acetone, followed by a 10-minute ultrasonic bath in isopropyl alcohol (IPA) at 50 °C, and lastly a submersion in ultrapure water. Finishing the cleaning process, the substrates were dried with N_2 jetting. Later, for the deposition, the substrates were submitted to an Ultraviolet Ozone surface activation step with a lamp-substrate distance of 4.5 cm in a PSD-UV Novascan for 15 minutes.

For the spin coating deposition (WS-650MZ-23NPPB from Laurell Technologies) the solution was filtered through a 0.20 µm hydrophobic polytetrafluorethylene (PTFE) filter and the parameters used were: 35 seconds at 3000 rpm and an acceleration of 2000 rpm/s for each layer, followed by a 5-minute annealing at 400 °C in atmospheric conditions, with a humidity around 40%, between layers, and a final annealing of 1 hour in similar conditions. The substrates were blown with N_2 before each layer deposition to ensure the removal of any impurity.

The films were characterized chemically resorting to FTIR spectroscopy to ensure the elimination of organic residues and formation of the oxide film, optically and electrically using UV-Vis-NIR spectroscopy and hall effect, respectively, and their thickness and visual aspect (deposition quality, amount of impurities) analysed via ellipsometry for the former and optical microscopy for the latter.

The FTIR measurements, similarly to the measurements taken for the solutions, employed an ATR sampling accessory to obtain a spectrum in the range of 4500-525 cm^{-1}.

For the optical characterization, the samples were analysed by a Perkin Elmer lambda 950 UV/VIS/NIR spectrophotometer. The Transmittance (T%) spectra were obtained in the range from 250 nm to 800 nm with a 1 nm step. Later, in order to obtain Reflectance (R%) information to determine Absorbance (A) for the bandgap calculation, further spectroscopy studies were taken in a Shimadzu UV-3101PC UV-Vis-NIR Scanning Spectrophotometer resorting to an integrating sphere to obtain both the Total Reflectance and Total Transmittance.

The films thickness was determined by spectroscopic ellipsometry (Horiba Jobin Yvon, UVISEL DH10) on the films deposited on the silicon wafers, using two different energy ranges 0-59-6.5 eV and 1.5-5 eV. The data was modulated in DELTAPSI software, the fitting done pursuing the lowest error function (χ^2), (fitting and results present in annex C).

Optical microscopy (Olympus BX51 Microscope) using 50x, 100x, 200x and 500x amplification was employed as a supplementary characterization technique mainly to ensure the quality of the spin coating deposition, ensuring an adequately low enough number of defects in all the samples analysed.

Before the electrical characterization, aluminium contacts had to be evaporated on top of the film. The electrodes were deposited using a thermal evaporator in a Van der Pauw geometry with 80

nm of thickness, obtaining 4 samples for each thin film. Electrical characterization by Hall effect measurements (nanometrics) using Van der Pauw geometry followed. A constant magnetic field of 0.51 T was obtained. Each sample underwent 2 cycles, with an integration time of 1s and a delay time of 1s.

2.3. **Inkjet Implementation**

For the inkjet deposition was chosen the optimized sample, based on Z value, electrical properties, and eco-friendliness. Considering these conditions, solution and thin films based on ETH(80%)/EG(20%) were selected. Firstly, the solution was filtered using a 20 µm PTFE filter before filling the cartridge (Fujifilm Dimatix S-class). The initial test in inkjet printing (PiXDRO LP50 printer) was to assure the adequate formation of droplets. Once an ethanol-based solution was used the drops were not particularly big, however, it was possible to remove tailing and secondary drops, by manipulating the pulse shape values.

Unlike with spin coating, for the thin films deposition only Corning glass substrates were used to deposit by inkjet printing with the same UV/Ozone pre-treatment. Other parameters including a printhead height (z) of 0.3 mm and printing speed of 150 $mm.s^{-1}$ were established. Then, the printing was optimized by varying DPIs (drops per inch), from 100 to 1200 DPI's, changing the annealing and post annealing temperature, the number of layers (1 or 2) and the UV/Ozone treatment between layers.

The resulting films were observed by the optical microscope (Olympus BX51 Microscope), using 50x and 100x amplification for printing quality analysis. Lastly, the samples were taken to the profilometer (Bruker DetakXT) to assess their topography and thickness using a 2 µm stylus with a resolution of 0.055 µm.

3. Results and Discussion

This chapter summarizes the results obtained for the different solutions and thin films deposited both by spin-coating and inkjet printing.

3.1. Solutions Characterization

3.1.1. FTIR analysis

Understanding the chemical composition of the precursor solutions is paramount. The chemical bond analysis, resorting to Fourier Transform Infrared Spectroscopy (FTIR), for the different EG concentration (V/V) solutions performed using the ATR accessory from 4500-525 cm^{-1} is presented in Figure 3.1. The region marked with 1 (3600 – 2700 cm^{-1}) represents the peaks related to the organic compounds of the solvent, present in both Ethylene Glycol and 2-ME.

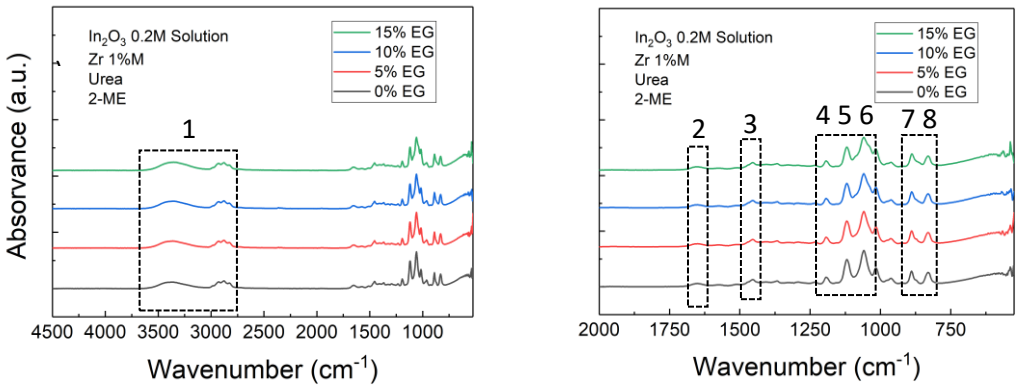

Figure 3.1- FTIR Spectra of 2-ME solutions a) range 4500-525 cm^{-1} b) range 2000-525 cm^{-1}

All the peaks are presented in Table 3.1 for further analysis. There are more peaks from the organic solvent presented, which will be analysed further. Peaks 2 (1650 cm^{-1}) and 3 (1456 cm^{-1}) can be attributed to C=O and C-N bond respectively, both from urea. Peaks 4 to 8 are also organic compounds and are from 2-ME solvent. Also, to note that the chemical composition of the solutions doesn't change with the EG concentration. Full spectra for the precursors and solvents can be viewed on annex A.

Table 3.1- Characteristic absorbance peak and corresponding chemical bonds and respective vibrational modes for the InO_x Zr-doped solution in 2-ME

Number	Wavenumber Peak (cm^{-1})	Vibrational Mode	Chemical bond	Reference
2	1650	Stretching	C-O	[45]
3	1456	Stretching	C-N	[46]
4	1190	Stretching	C-O	[45]
5	1120	Stretching	C-O	
6	1060	Stretching	C-O	
7	889	Bending	C-H	
8	830	Bending	C-H	

3.1.2. Viscosity

Given the inkjet deposition intent, the viscosity measurements are crucial. The viscosity and Z-value of the solutions were obtained and considered in order to determine the compatibility of each solution to inkjet printing, with Z-value within 1 and 10[41]. Figure 3.2 presents viscosity and Z-value of the different solvent solutions and the EG concentration. The Z-value calculations are presented in

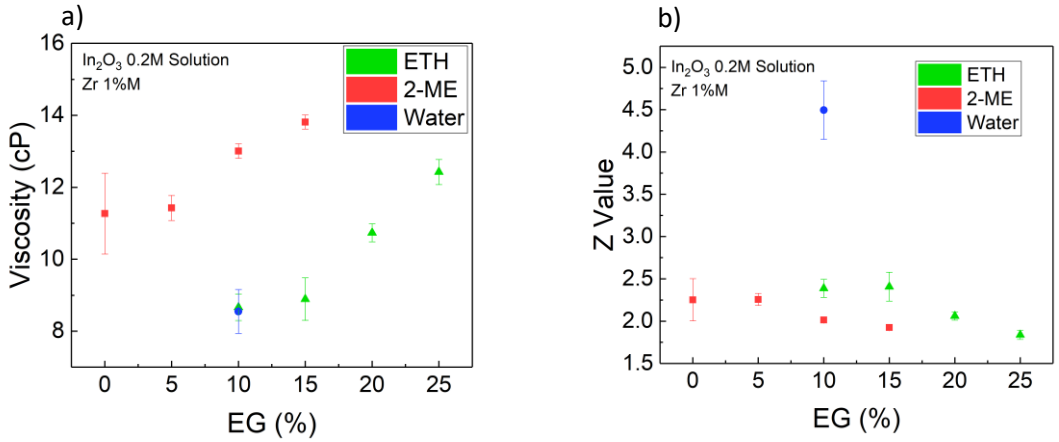

Figure 3.2- a) viscosity and b) Z-value for the 2-ME, ETH, and water solvents

NOTE for black and white printing: 2-ME solution is represented by squares, ETH by triangles and Water by circle.
annex B.

Based on figure 3.2 a) the increase in EG concentration (V/V) has a positive effect in the viscosity of the solution, regardless of the solvent adopted. Moreover, for similar EG concentrations, 2-ME solutions present a higher viscosity compared to ethanol, which is to be expected, as 2-ME presents a longer polymeric chain being more viscous than ETH.[47] Water on the other hand presents a similar viscosity for the same EG concentration as ethanol, which, considering the physical properties, such as surface tension as well as the molecular structure differences, was surprising . Figure 3.2 b) shows the Z-value, a more relevant value for inkjet printing, which is this case. Unlike with the viscosity, the EG concentration has a much lower influence, showing just a slight decrease in Z-value as EG concentration increases, both for 2-ME and ETH. A small difference is also present when comparing,

considering the same EG concentration, 2-ME to ethanol as solvents, where ethanol shows a slightly higher Z-value compared to similar 2-ME solution; water however has a more noticeable difference when compared to the other solvents, the Z-value it presents is relevantly higher despite being within the optimal range, 1<Z<10.[41]

3.1.3. Solubility assessment and stability

Before deposition, a last and very important analysis takes place. To proceed to deposition, it is important that the solution is uniform and well dissolved, not only to ensure the solution combustion synthesis occurs as planned, but also to ensure uniformity of the film. Figure 3.3 shows different solutions and solution attempts and allows to conclude which were adequate to follow up with deposition.

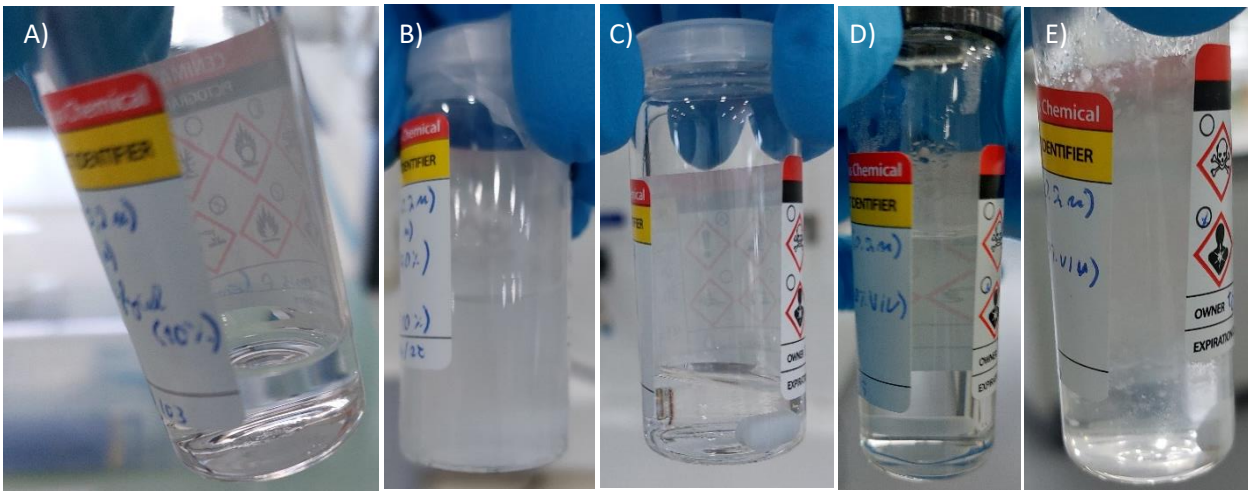

Figure 3.3- A) 2-ME solvent, 10% EG solution B) ETH solvent, 10% EG with urea C) ETH solvent, 10% EG, without Uuea D) Water solvent, 10% EG, without SDS E) Water solvent, 10% EG, with SDS.

As can be seen in figure 3.3, there were no dissolution problems for 2-ME. Ethanol was the solvent for the following solutions. In this case, the urea had trouble dissolving despite being within the solubility limits for ethanol.[48], [49]. A solution without urea was attempted, and resulted in a clear, well dissolved solution, so it was employed. Lastly, ultrapure water was used as a solvent, and, using the same components as the ethanol solution preceding it, the dissolution was achieved. However, due to problems with the deposition, attributed to differences in surface energy, SDS was added to mitigate such issue. This, however, resulted in a poor dissolution. After the study, ethanol was chosen since it allowed good dissolution and showed potential for adequate thin films, whilst being more sustainable than 2-methoxyethanol which is carcinogenic.

3.1.4. Thermal characterization

To evaluate the decomposition of metal oxides a thermal characterization was performed for the most promising solution concerning their implementation in inkjet printing. Figure 3.4 show both the thermal gravimetry (TG) and the differential scanning calorimetry (DSC) results for the Zr (1%M) doped In_2O_3 precursor solution with a concentration of 0.2M and a EG concentration (V/V) of 20% in ETH.

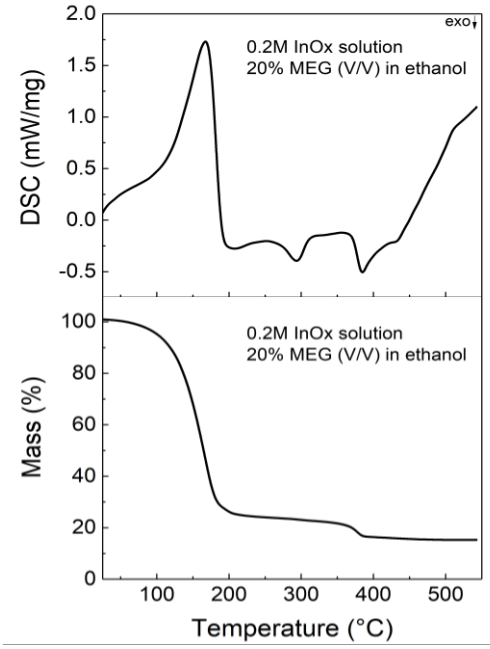

Figure 3.4- DSC-TG analysis of powder for a Zr-doped In_2O_3 20% EG (V/V) in ethanol solution.

From Figure 3.4 an endothermic peak in noticeable at 167°C, it is accompanied by a mass reduction, this can be a result of evaporation of solvent since we have a mixture of two solvents which boiling points are 78.2°C and 197°C for ethanol and ethylene glycol, respectively. As temperature increased there are two exothermic peaks, at 293°C and 385°C, for the latter temperature the sample shows a slight mass loss. This indicates that, for complete formation of the thin film, the minimum required temperature is 385°C. Given these results, the annealing temperature of 400°C proves adequate. None of the exothermic peaks is particularly intense, which, considering the lack of a proper fuel like urea could be expected.

3.2. Spin Coated thin films characterization

As a part of the optimization process, different factors, like indium precursor concentration, number of layers, solvent employed and EG quantity were studied, and their effects regarded for optical, chemical, physical and electrical properties.

3.2.1. Indium precursor Concentration influence

For this parameter, two different concentrations were studied, 0.1M and 0.2M.

3.2.1.1. Chemical Analysis

Figure 3.5 presents the thin films FTIR plot for both concentrations.

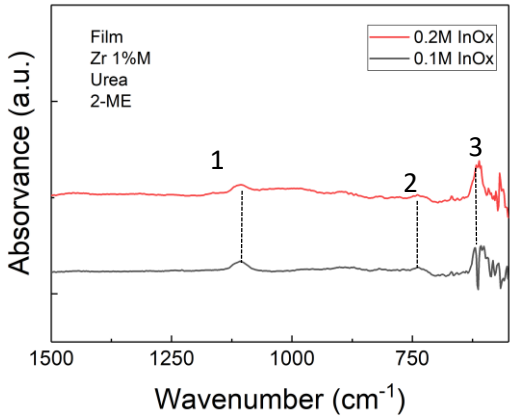

Figure 3.5-FTIR Spectra for Zr-doped In_2O_3 0.1M and 0.2M concentration thin films

From Figure 3.5 one can conclude that the indium precursor concentration does not have a large impact in the film formation. As to be expected, on the chemical properties, both solutions produced similar thin films. The main peaks are shown in Table 3.2.

Table 3.2- Characteristic absorbance peaks and associated vibrational modes of the corresponding chemical bonds.

Number	Wavenumber Peak (cm^{-1})	Vibrational Mode	Chemical bond	Reference
1	1108	Transverse Optical Stretching	Si-O	[38]
2	740	Stretching	In-O	
3	620	Bending	In-O	

Furthermore, Figure 3.5 allows the conclusion that the In_2O_3 thin film was successfully formed, as proven by the peaks at 740 cm^{-1} and 620 cm^{-1} indicating the formation of In-O bonds. Moreover, comparing either spectrum to the solution ones, as shown in Figure 3.6, the decrease in organic peak in the region noted with the number 4 results from the evaporation of the solvent as expected.

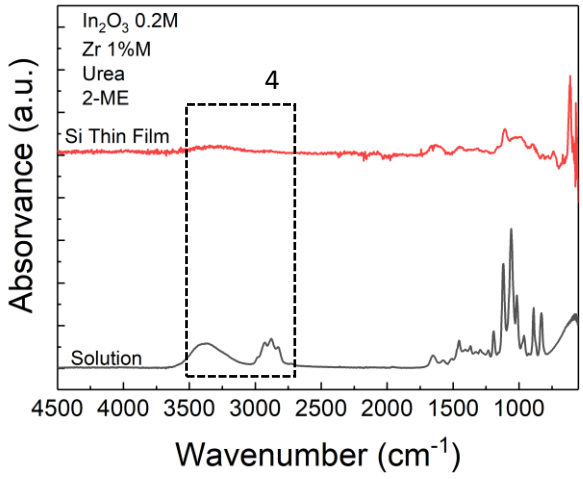

Figure 3.6- FTIR spectra for Zr-doped In2O3 solution and thin film

3.2.1.2. Thickness effect

The films thickness was determined, as aforementioned, by ellipsometry. The thickness affects both the electrical properties (in general, the thicker the film, the lower the resistivity, a desirable effect) as well as the optical properties – transparency - which is also affected, however, in this regard, the more desirable properties appear for thinner films (a thinner film is more transparent). Figure 3.6 shows how the indium precursor concentration affects the film thickness. In both cases, the film was deposited on a Si substrate, and both had 8 layers deposited. The difference is clear, higher concentration results in thicker films.

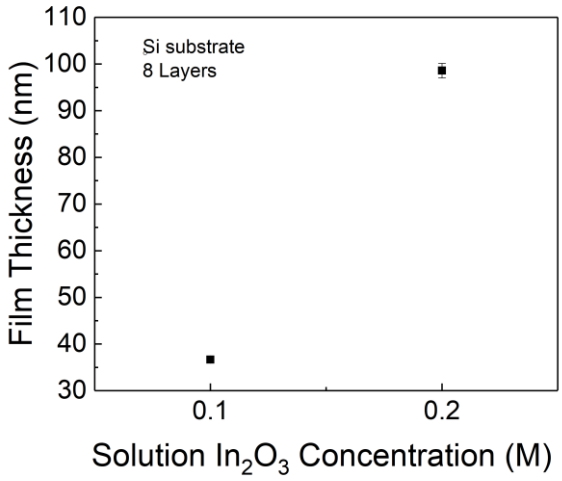

Figure 3.7- Thickness of Zr-doped films with different In_2O_3 molar concentration

3.2.1.3. TCOs electrical properties

The electrical properties were obtained by Hall effect measurements, which can determine not only the resistivity, but also the Hall coefficient, carriers' mobility, and concentration. Table 3.3 summarizes the electrical properties of 8-layer films deposited on Corning glass, for both precursor concentrations. There is a noticeable difference in the resistivity of both films. The 0.2M film has better performance for all different properties, Hall coefficient and mobility, and in the carrier concentration. Based on Table 3.3, 0.2M was the concentration used for the rest of the work. Table 3.3 also presents the requirements, sheet resistance and carrier density, for both touch screen electrodes (TSE) and thin film solar cells (TFSC) and large area flat panel displays(LAFPD)[50].

Table 3.3-Hall effect measurements of the Zr-doped In_2O_3 thin films annealed at 400° C and produced with different molar concentrations.

InO_x precursor solution concentration (M)	Resistivity		Hall		Carrier concentration	
	Sheet ($\times 10^4\ \Omega$.sq)	Bulk ($\times 10^{-1}\ \Omega$.cm)	Coefficient (m^2/C)	Mobility ($cm^2/V.s$)	Sheet ($\times 10^{13}\ cm^{-2}$)	Bulk ($\times 10^{18} cm^{-3}$)
0.1	248	90.768	-51.6	0.21	-1.21	-3.306
0.2	0.9335	0.920	-1.96	2.10	-31.93	-32.419
TSE	0.4-0.7	-	-	-	-	-100-1000
TFSC/LAFPD	0.001	-	-	-	-	-100-1000

3.2.2. Influence of the number of layers

For this study 8 and 10 layers were deposited from the same solution, like determined before, with an indium precursor concentration of 0.2M. No chemical differences were noted (annex C), as to be expected, so only the thickness and electrical properties were analysed.

3.2.2.1. Thickness

Like before, the thickness was measured in Si substrates by ellipsometry. Unlike with the variation in indium precursor concentration, the study on the number of layers resulted in a smaller difference, 8 layers presented a thickness of 98.5 ± 1.5 nm whereas 10 layers showed slight increase, 105.8 ± 0.89 nm, which was not significant, considering an increase of 25% in the number of layers resulted in an increase of 7.4% in thickness.

3.2.2.2. Electrical properties

The Hall effect measurements, concerning the number of layers, are shown in Table 3.4. As expected, increasing the number of layers, by increasing the thickness, reduces the resistivity of the film. The carrier concentration remains quite similar. The Hall mobility, however, presents the biggest difference, being the main factor for the resistivity reduction. However, and despite the slight improvement in the electrical performance, 8 layers were chosen over 10 layers for the remaining work, the reduction in resistivity is within the same order of magnitude. Additionally, increasing the number of layers contributes to an increase in both usage of material as well as time required for the deposition, and introduces more interfaces, which are the most susceptible areas to introduction of defects.

Table 3.4-Hall effect measurements of Zr-doped In_2O_3 thin films annealed at 400° C and produced with different number of layers.

Number of layers	Resistivity		Hall		Carrier concentration	
	Sheet ($\times 10^4\ \Omega$.sq)	Bulk ($\times 10^{-1}\ \Omega$.cm)	Coefficient (m^2/C)	Mobility ($cm^2/V.s$)	Sheet ($\times 10^{13}\ cm^{-2}$)	Bulk ($\times 10^{18} cm^{-3}$)
8	0.9335	0.920	-1.96	2.10	-31.93	-32.419
10	0.6354	0.672	-1.82	3.00	-34.44	-32.554
TSE	0.4-0.7	-	-	-	-	-100-1000
TFSC/LAFPD	0.001	-	-	-	-	-100-1000

3.2.3. Ethylene Glycol volume influence in the film properties

Presented here are the EG volume effect for 2-ME solution based thin films. Despite being a compound added to the solution, to control the physical properties, chemically it does not present significant changes as is presented in Annex D. The same study for ETH based solutions is presented further ahead in this work.

3.2.3.1. Thickness

As presented before, EG concentration influences the viscosity of the solution, which, in turn, is expected to result in thickness variations. Figure 3.8 shows the results of the ellipsometry measurements.

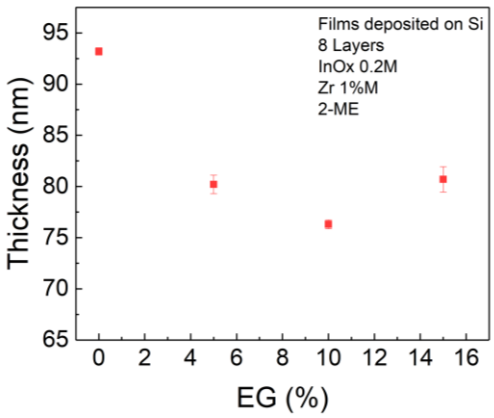

Figure 3.8- Thickness of 2-ME based films deposited on Si annealed at 400 °C, with different EG volumes.

From figure 3.8, it becomes apparent that increasing the EG contributes to the decrease in thickness of the films, up to 15% EG concentration (V/V). Despite the increase in viscosity, that, maintaining the other properties the same, should result in thicker films, there is an increase in density as well as a slight increase in the boiling temperature.[51], [52] The increase in boiling temperature reduces evaporation during the spin coating process. This evaporation is responsible for an increase in viscosity during the spin coating process, reducing it will reduce the thickness of the films. Furthermore, an increase in density results in thinner films.[53] However, another explanation for the result showed is the inadequacy of the model used in the ellipsometer. As the EG concentration increases the model might become unfit for these conditions.

3.2.3.2. Electrical properties

Like with the previous studies, the electrical properties are the most relevant ones. Table 3.5 synthesizes the hall effect measurements of the 2-ME, 8-layer thin films, for EG concentrations from 0% (V/V) to 15% (V/V). Table 3.5 shows that an increase in EG concentration has a slight negative effect on the electrical properties, however, in the studied range, the difference is not significant. Either concentration would be suitable for the desired application.

Table 3.5-Hall effect measurements for 2-ME based Zr-doped In_2O_3 thin films for different EG concentration.

Percentage of EG (V/V)	Resistivity		Hall		Carrier concentration	
	Sheet ($\times 10^4\ \Omega$.sq)	Bulk ($\times 10^{-1}\ \Omega$.cm)	Coefficient (m^2/C)	Mobility ($cm^2/V.s$)	Sheet ($\times 10^{13}\ cm^{-2}$)	Bulk ($\times 10^{18} cm^{-3}$)
0%	0.9335	0.934	-1.96	2.10	-31.933	-31.933
5%	2.3813	1.910	-2.83	1.20	-22.547	-28.113
10%	2.2403	2.014	-2.27	1.02	-27.890	-31.023
15%	5.7440	4.630	-3.42	0.60	-18.590	-23.065
TSE	0.4-0.7	-	-	-	-	-100-1000
TFSC/LAFPD	0.001	-	-	-	-	-100-1000

3.2.4. Solvent study

After completing the 2-ME based studies, given the toxicity of such solvent, the search for alternative solvents was followed. For the alternatives, greener solvents were preferable, such as water and ethanol, however water was unusable as a solvent when attempting to deposit it. Following the previous studies, EG was employed to control viscosity for inkjet application, for ETH, in higher volumes.

3.2.4.1. Thickness

The ellipsometry results are presented in Figure 3.9 for both ETH and 2-ME based thin films. The EG concentration presents a similar influence in both solvents. It had, however, different orders of magnitude. In both cases, the increase in EG concentration resulted in thinner films. In the 2-ME based solutions, despite the increase in viscosity, due to an increase in density as well as a slight increase in boiling temperature and surface tension, a higher amount of solution is expelled over the edge of the substrate for EG concentrations up to 10%. For 15% these effects are less prevalent and the increase in viscosity was responsible for a slightly thicker film. Since the difference in ETH and EG's boiling point is greater than that between 2-ME and EG, the addition of EG to the ethanol solution showed a more prevalent effect in reducing the film's thickness, up to a concentration of, at least, 25%, with a greater difference in thickness when compared to the 2-ME solutions.

For ETH based solutions, the resulting films presented a higher thickness for similar EG concentrations when compared to the 2-ME equivalent film. Such difference can be explained by the lower boiling point of ethanol that, during the spin coating might evaporate at a higher rate, resulting in a higher viscosity through the deposition process and fewer losses due to solution being expelled from the side of the substrate. [53]–[55]

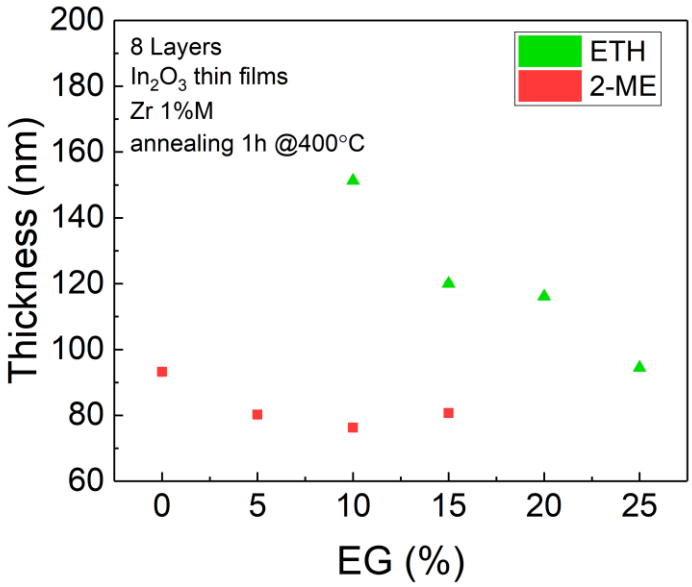

Figure 3.9- Thickness of both 2-ME and ETH based Zr-doped In2O3 thin films with different EG concentration.

NOTE for black and white printing: 2-ME films are represented as squares and ETH film as triangles.

3.2.4.2. Electrical characterization

To complete the study, the Hall effect measurements were taken and are shown in figure 3.10. and in Table 3.6. the exact measurements can be analysed. Just like with 2-ME, increasing the EG

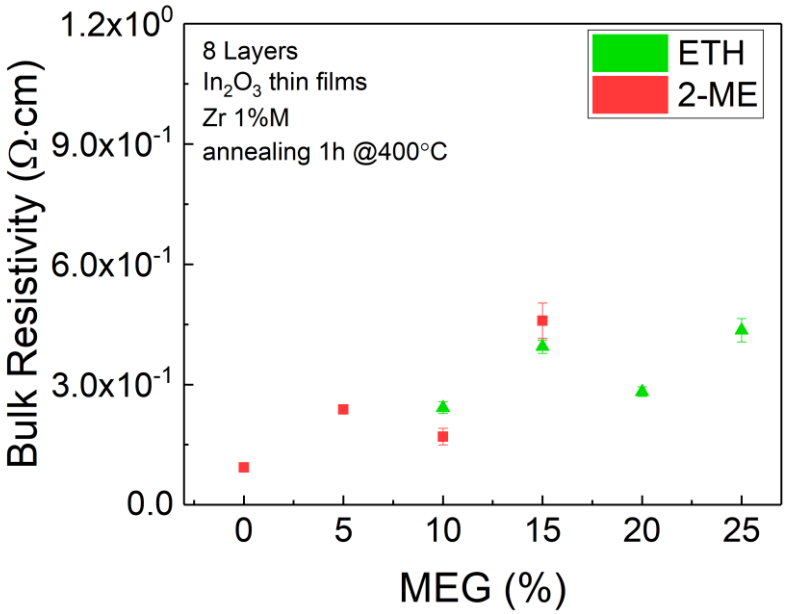

Figure 3.10-Sheet resistivity of Zr- doped In_2O_3 thin films for 2-ME and ETH samples

NOTE for black and white printing: 2-ME films are represented as squares and ETH film as triangles.

concentration in ETH based solutions results in a slight increase in the resistivity. Exceptions to this appear in thin films from both solvents, for 10% EG concentration in 2-ME based film and 20% for ETH film, which can be due to ambient factors, such as a difference in humidity or another condition during deposition. Another factor, the solvent employed, also shows an influence in the resistivity of the thin films, with ETH films, for the same EG concentrations, presenting a lower sheet resistance, however, this does not translate to the bulk resistivity. Considering the results, the ETH with 20% EG quantity (V/V) ink will be the employed solution for the inkjet printing.

In Figure 3.10, the bulk resistivity for Zr-doped In_2O_3 thin films is presented for 2-ME solution, with an EG concentration between 0%(V/V) and 15%(V/V) with a 5% interval. Besides, it also presents the bulk resistivity for Zr-doped In_2O_3 thin films from ETH solution, however, for this solution, the EG concentration stands between 10%(V/V) and 25%(V/V), also with a 5% interval between concentrations studied. These same results, as well as the sheet resistance, Hall coefficient and mobility and Carrier concentration in bulk and sheet for the same films are summarized in Table 3.6.

Table 3.6-Hall effect measurements for all the Zr-doped thin films from both 2-ME and ETH solutions, with EG concentrations from 0% to 15% for 2-ME solutions and from 10% to 25% for ETH solutions.

Percentage of EG (V/V)	Solvent	Resistivity		Hall		Carrier concentration	
		Sheet ($\times 10^4\ \Omega$.sq)	Bulk ($\times 10^{-1}\ \Omega$.cm)	Coeffi-cient (m^2/C)	Mobility ($cm^2/V.s$)	Sheet ($\times 10^{13}\ cm^{-2}$)	Bulk ($\times 10^{18} cm^{-3}$)
0%	2-ME	0.9335	0.934	-1.96	2.10	-31.933	-31.933
5%	2-ME	2.3813	1.910	-2.83	1.20	-22.547	-28.113
10%	2-ME	2.2403	2.014	-2.27	1.02	-27.890	-31.023
10%	ETH	1.7418	2.421	-1.41	0.82	-45.398	-32.645
15%	2-ME	5.7440	4.630	-3.42	0.60	-18.590	-23.065
15%	ETH	2.8585	3.945	-1.62	0.57	-39.300	-28.118
20%	ETH	2.4968	2.822	-1.75	0.70	-35.665	-31.570
25%	ETH	4.1470	4.355	-2.20	0.53	-28.415	-27.065

3.2.5. Optical analysis

The optical properties of the thin film are of the upmost importance, for the desired transparent electronic applications. This analysis is based on firstly a macroscopic observation to have a general idea of the transparency and of any evident defects. Secondly, a microscopic analysis allows to confirm the dimensions, extent of the defects and overall smoothness of the film, it also reveals any other defects previously unnoticeable. Lastly, UV-Vis-NIR spectroscopy is employed for in-depth understanding of the film's interaction with light of different wavelengths, assessing the transparency, and determining the bandgap.

3.2.5.1. Macroscopic analysis

In Figure 3.11 it is possible to note that, despite all films being transparent, there is quite a difference between the 2-ME based when compared to the ETH based ones. For the different depositions, the outside edge tends to present a bluer tint, this happens for all samples. The 2-ME samples present a narrower edge and for the ETH films, this edge narrows as the EG concentration increases, this might be due to the evaporation that occurs during the deposition. By increasing the boiling point, in the case of the ETH films, the film will evaporate at a lower rate, presenting a more uniform film. When it comes to the ETH films, these present a slight yellow tint in the middle that the 2-ME do not, they are more colour neutral. This property seems to be exclusively attributable to the solvent since the differences in EG concentration have no such effect in either solvent. Depending on the usage this might have to be addressed. When implementing in a solar panel, for example, considering the overall transparency it might not be an issue. Whereas for LCD implementation, it will require a colour adjustment, a slightly bluer backlight for example might counteract the issue.

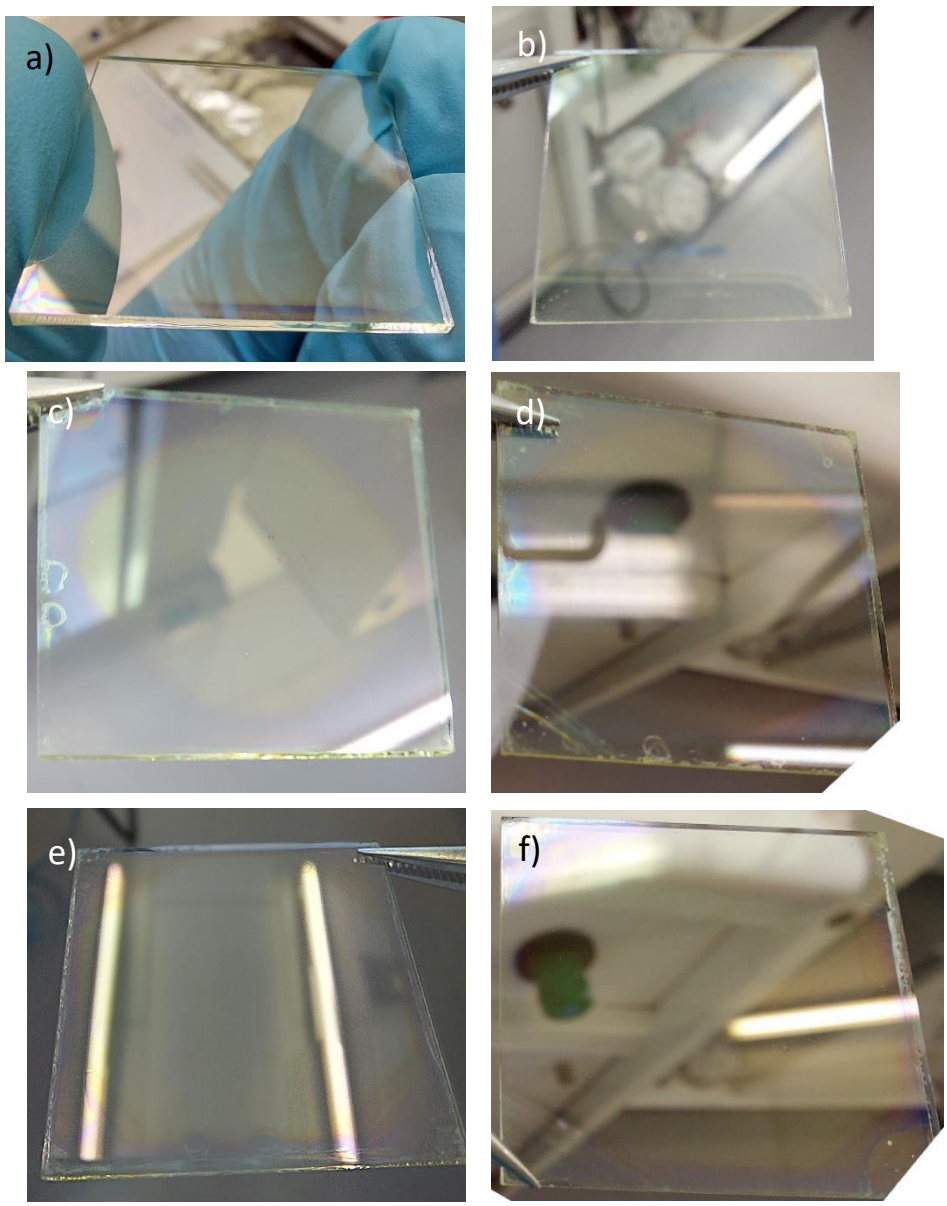

Figure 3.11- Photos of the Zr-doped In_2O_3 thin films deposited on the corning substrate: 2-ME a) 0% EG, b) 10% EG and ETH c)10% EG, d)15% EG, e)20% EG, f)25% EG.

NOTE: all thin films presented have 8 layers except e) which has 7 layers in the picture (note for scale: corning glass has 2.5cm side length)

3.2.5.2. Microscopic analysis

The uniformity of the film is an important parameter, however, during the deposition and annealing, the formation of bubbles might result in a material accumulation that will result in film defects. This risk and magnitude of defects naturally increases with the number of layers, each layer has potential to introduce defects onto the film. Other sources of defects could be dust that, despite blowing all the films between each layer through the spin coating step might still be present, or even an insufficient cleaning process or mishandling between the cleaning and the deposition. In this chapter different films will be analysed to draw conclusions about the impurities.

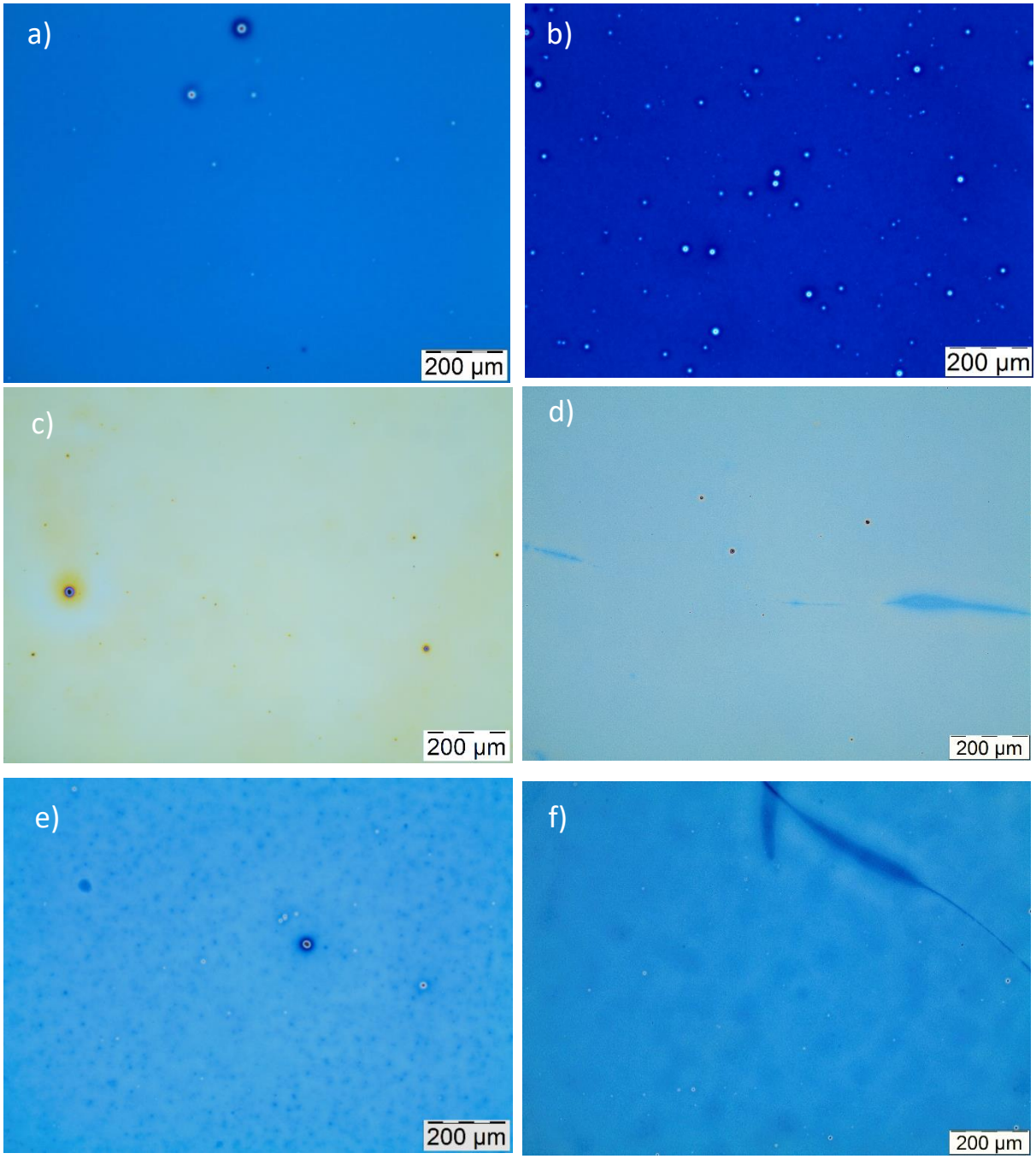

Figure 3.12- Zr-doped In2O3 thin film on Si substrate images under 50x ampliation with different solvents: 2-ME a) 0% EG, b) 10% EG and ETH c) 10% EG, d) 15% EG, e) 20% EG, f) 25% EG, all of the films were 8 layers

From analysing figure 3.12, it appears that ethanol-based films present fewer defects, with 10% EG 2-ME film (figure 3.12 a)) showing the most defects of all films, however it could be due to a particular batch. For ETH films with lower EG concentration (figure 3.12 c) and d)) these seem to present the smoothest films, showing just a few defects with the rest of the film appearing very even. As the EG concentration increases in the ETH films (figure 3.12 e) and f)) there appears to be a formation of a pattern of spots.

3.2.5.3. UV-Vis-NIR spectroscopy

To attest the transparency, a UV-Vis-NIR spectrometer (Perkin Elmer LS55) was employed, and the transmittance measured for wavelengths between 250 nm and 800 nm. The full spectrum analysis is presented in Figure 3.13.

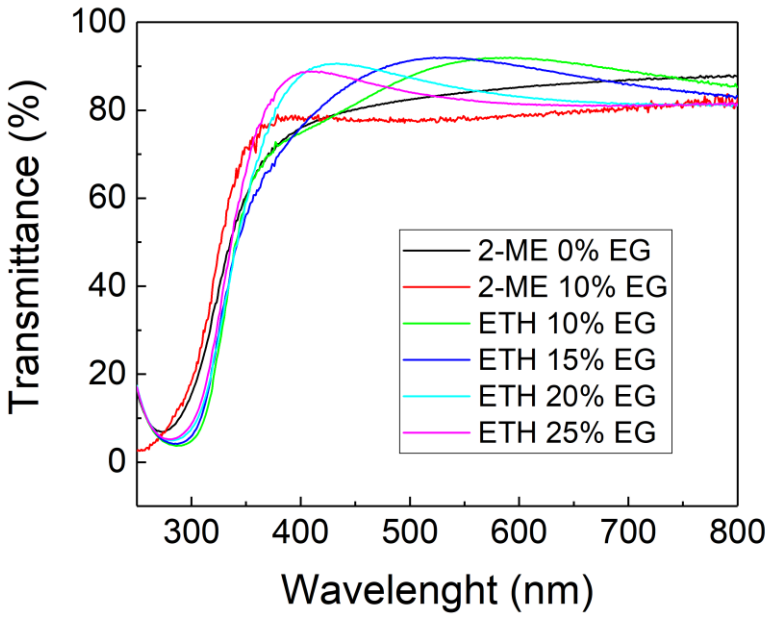

Figure 3.13-Spectroscopy analysis of Zr-doped In_2O_3 thin films from both 2-ME and ETH solutions, all thin films had 8 layers and were deposited in Si

Considering the spectra obtained, the differences in transmittance between the samples are not particularly significant, however, the condition of 2-ME with 10% EG showed the lowest transmittance. When both 2-ME and ethanol were used as solvent, the resulting films showed adequate transparency. The most relevant interval of the spectrum is the visible light, as such an average from 400 nm to 750 nm was obtained for comparison between the films. The results are presented in Table 3.7.

Table 3.7- Average Transmittance of Zr-doped In_2O_3 thin films over the visible range

Sample	Average transmittance (750nm-400nm)
2-ME	83.9%
2-ME 10% EG	78.9%
ETH 10% EG	84.3%
ETH 15% EG	87.8%
ETH 20% EG	83.0%
ETH 25% EG	83.2%

Lastly, based on the transmittance and reflectance, the optical bandgap for some thin films was calculated resorting to the Tauc's Plot. The methodology is explained in Annex E.

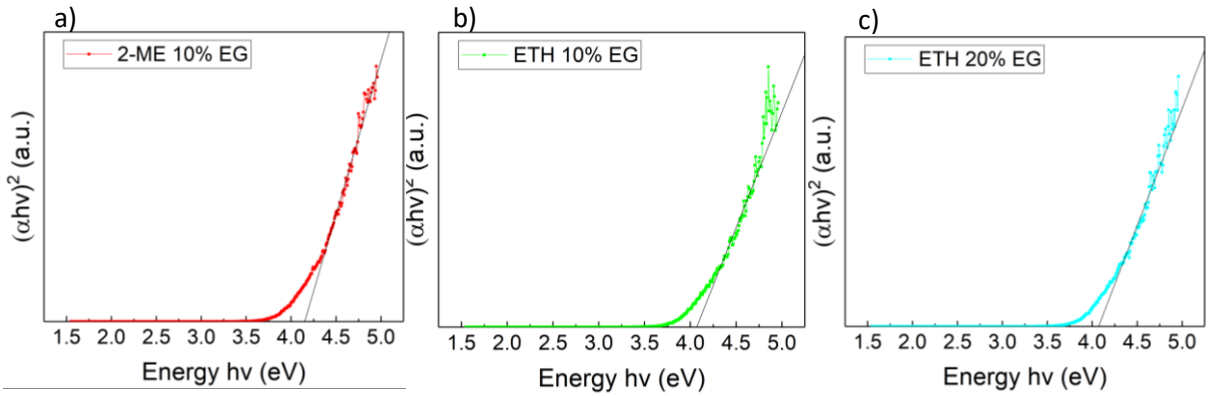

Figure 3.14-Tauc's plot for Zr-doped In_2O_3 thin films for: a)2-ME 10% EG b)ETH 10% EG and c)ETH 20% EG thin films.

The values for the bandgap are presented in Table 3.8, based on the fitting presented in Figure 3.14.

Table 3.8- Calculated values for bandgap of different thin films presented in Figure 3.14.

Sample	Bandgap (eV)
2ME 10% EG	4.15
ETH 10% EG	4.07
ETH 20% EG	4.07

The values presented in Table 3.8 confirm not only the transparency of all the thin films but also the influence of the solvents used in this case. The EG concentration has no influence in the bandgap and the difference between 2-ME and ETH is insignificant. And the bandgap values are within the expected value for In_2O_3 thin films (3.5eV-4.3eV).[56]

3.3. Implementation of Inkjet Printing for film deposition

Once determined the most suitable solution, inkjet implementation was followed. Firstly, and followed throughout, the formation of the drops had to be ensured, manipulating the wave pulse. Ethanol is a solvent with a low surface tension and viscosity (annex B), this meant the resulting drops were relatively small despite the EG addition to help combat the issue. Still, there was a formation of drops and elimination of any tailing drops, proving adequate for the deposition. The main parameters to consider where: UV pre-treatment of the substrate before printing, number of DPIs (dots per inch) for printing and number of layers of the thin film. All depositions used a distance to the substrate (z) of 0.3 mm.

3.3.1. UV treatment

The first test conducted In the inkjet Implementation was the UV treatment of the substrate.

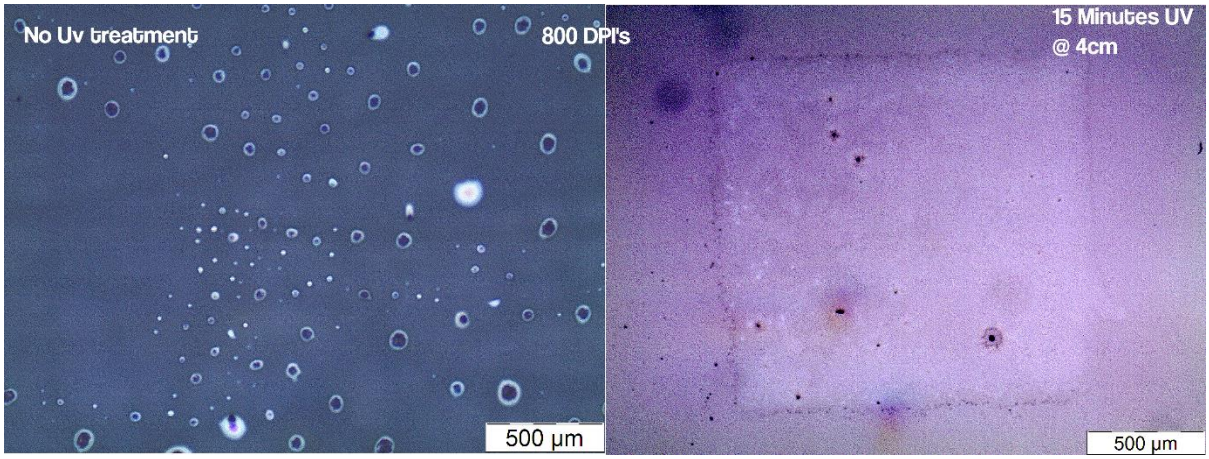

Figure 3.15- 800 DPI printed film in a) no UV treated substrate b) substrate subjected to 15 min UV treatment at 4 cm.

As shown in figure 3.15, without the UV pre-treatment of the substrate, the drops do not spread, therefore making it impossible to create a film. But, with a 15-minute UV pre-treatment, the desired effect was reached, and the drops spread and join each other forming a thin film. Considering the results of this test, all the subsequent films were deposited on a Corning glass substrate after undergoing a 15-minute UV pre-treatment.

3.3.2. DPI study

Afterwards, the DPI study was conducted, the goal was to form uniform thin films. The study was performed from 100 DPIs to 1200 DPIs. The films underwent an annealing of 10 minutes at 130°C after the deposition.

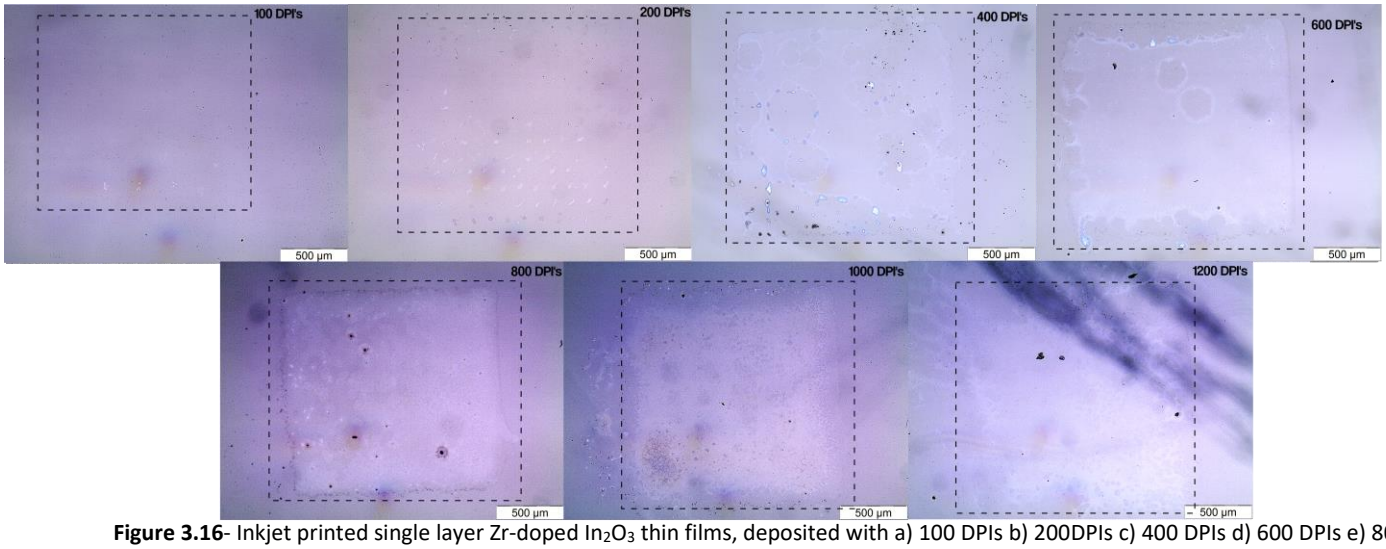

Figure 3.16- Inkjet printed single layer Zr-doped In_2O_3 thin films, deposited with a) 100 DPIs b) 200DPIs c) 400 DPIs d) 600 DPIs e) 800 DPIs f) 1000 DPIs g) 1200 DPIs

Figure 3.16 summarizes the DPI study. At 100 DPIs, It Is only possible to discern a few drops, for an unknown reason the drops did not spread throughout the substrate. 200 DPIs resulted in a square forming, however, the spread resulting from this resolution was not good enough to result in a film which resulted in printing a dotted square. From 400 DPIs to 800 DPIs the results showed the

most promise. 400 DPIs and 600 DPIs still show a few circles where film formation did not occur despite an even film outside of such circles. 800 DPIs, despite a few imperfections in the films, showed adequate spread and formed a thin film. Higher DPIs, 1000 DPIs and 1200 DPIs resulted in cracked films, most likely due to accumulation of ink which results in a release of gaseous products during annealing.

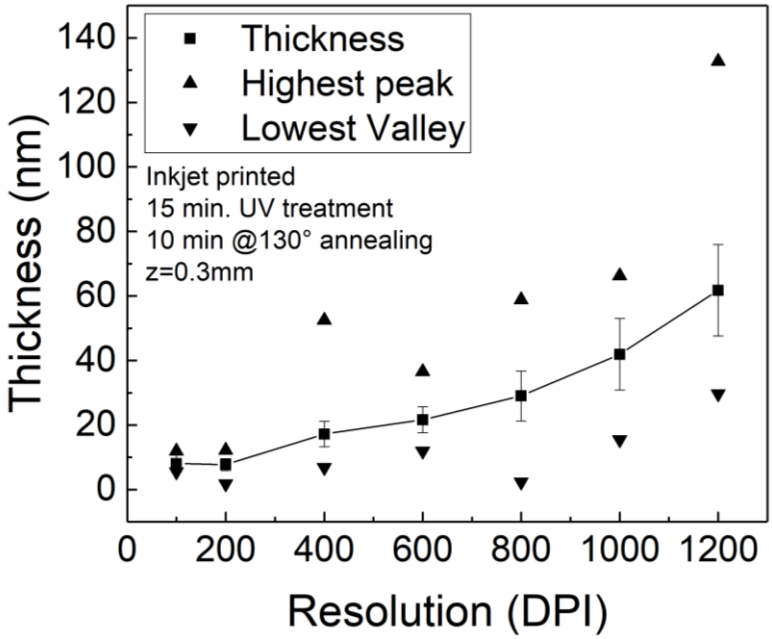

Figure 3.17-Average thickness, highest peak and lowest valley for inkjet printed samples with a resolution ranging from 100 to 1200 DPIs.

Analysing Figure 3.17 a clear trend allows to conclude that an increase in resolution results in thicker films. Moreover, indicated by the error bars, the roughness of the films tends to increase with the resolution. Lastly, 600 DPIs presents the more uniform films across the analysed area, with both the highest peak and lowest valley being the closest to the average thickness. Additionally, 1200 DPIs shows a non-uniform spread throughout the length of the measurement, presenting an accumulation of ink. Full results are shown in Annex F.

3.3.3. Number of layers study

Once single layer films were successfully printed, the next step was increasing the number of layers.

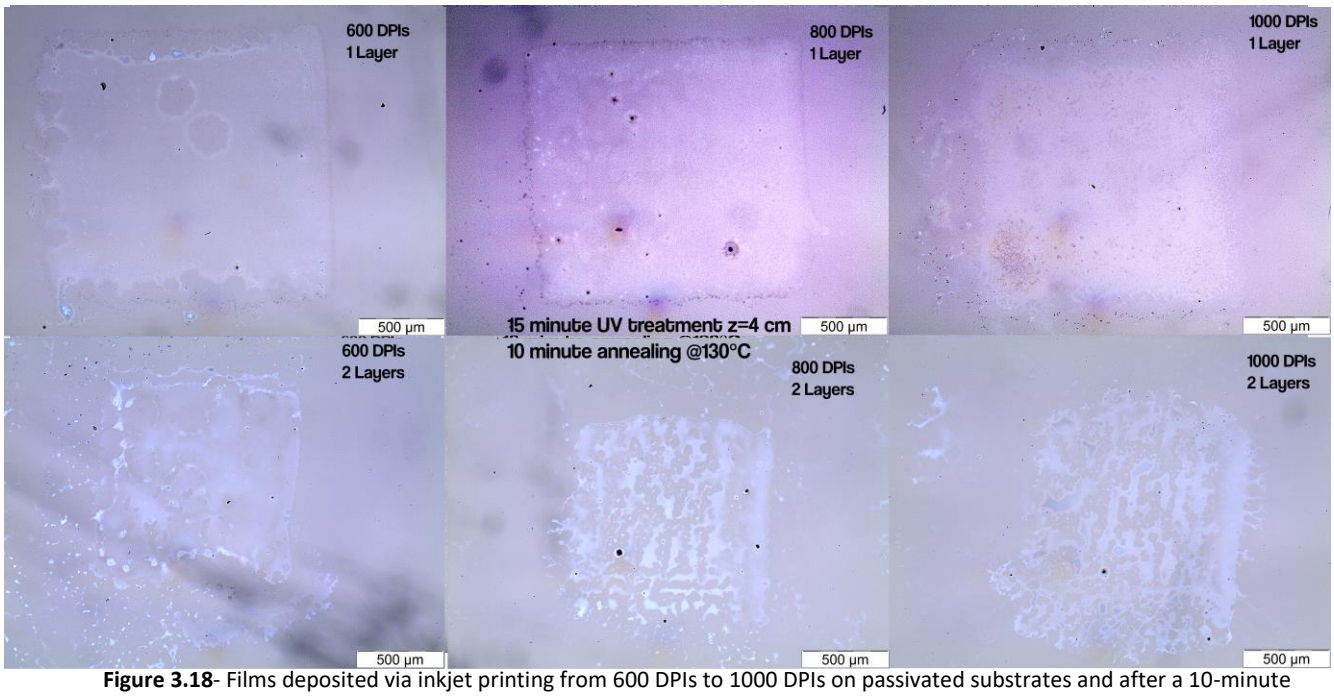

Figure 3.18- Films deposited via inkjet printing from 600 DPIs to 1000 DPIs on passivated substrates and after a 10-minute annealing @130°C for both layers.

Figure 3.18 presents the results of the layer study. The single layer films, displayed in the upper row, were already discussed in chapter 3.3.2. The substrates were subjected to a UV pre-treatment as before and UV treatment between layers besides a 10-minute annealing at 130°C between layer and after the second layer, for this last layer it underwent a post annealing for 30 minutes at 300°C. For the 2-layer films, the results are not as promising, yet, as the single layer ones. For 800 DPIs and 1000 DPIs, the ink adhesion seems insufficient despite UV treatment between layers. It can be due to a poor adhesion on the first deposition, mostly due to some form of malfunctioning along the process since the parameters were the same as the ones for the single layer (top row). Another reason can be the second layer not adhering well to the top of the first, problem that did not occur for the spin coating depositions, and that can be attributed to the annealing at 130°C. For 600 DPIs, part of the film is more uniform. However, the shape is very poorly defined, raising an issue still.

4. Conclusions and Future Perspectives

This dissertation's main goal was to study and optimize solution-based Zr doped-InO_x for TCO applications. Furthermore, the approach employed focused on sustainability, with the study of ethanol (ETH) as a solvent and inkjet printing as the deposition method, an additive process, removing the need for masks and etching and making the process less dependent on expensive industrial techniques.

Firstly, 2-methoxyethanol (2-ME) was employed as a solvent for the initial study of the effects indium precursor concentration, the number of layers, and ethylene glycol (EG) concentration had in the electrical properties. Using urea as fuel, the better concentration was 0.2M when compared to 0.1M. Regarding the number of layers, 8 and 10 layers were the chosen values, and the result showed no significant difference. This led to the adoption of 8 layers, since it not only uses less material and requires less time (a bigger issue in industrial applications when compared to research) but also reduces the number of interfaces, which leads to a reduction in the potential number of defects. Lastly, EG concentration was varied from 0% (V/V) to 15% (V/V) in 5% (V/V) steps and, despite the negative effect it had in the conductivity of the films, it was not significant enough to offset the influence it had on the viscosity, a fundamental property for inkjet implementation.

After the first results and achieving promising conductivity for the desired application, optimizing the process for greener solvents followed. Water and ethanol were the solvents of choice. For the water solution, it would not adhere to the substrate and the addition of a surfactant (SDS) to help with the deposition lead to an unusable solution, given the dissolution issues. The ETH solution had issues dissolving urea. The solution was to use, in the ETH solution, EG not only regarding viscosity but fuel as well, the exothermic reaction would not be as pronounced, but still presented adequate thin films. Since ethanol is a more volatile and less viscous solvent when compared to 2-ME, the EG concentration studied was higher (10% (V/V) to 25% (V/V)). Once again, the electrical effect of the EG was minimal, so the concentration chosen was 20% (V/V).

Table 4.1 -Bulk Resistivity of multiple TCOs with different dopants and from different deposition methods

Note: the first sample of my work, is the one presenting the best electrical properties (2-ME 0%(V/V) EG 10 layers) Whilst the second sample is the one employed by the inkjet (ETH 20%(V/V) EG 8 layers)

Year	TCO	Dopant	Annealing temperature (°C)	Deposition Method	Bulk resistivity ($\times 10^{-1}$ Ω.cm)
2017 [34]	In_2O_3	Sn (10 wt%)	300	Sputtering	0.0025
2018 [35]	In_2O_3	Ce (3.7%)	500	Spin-Coating	0.0129
2018 [35]	In_2O_3	Sn (1.36%)	500	Spin-Coating	0.0242
2018 [36]	In_2O_3	Ti (0.3M)	450	Spin-Coating	0.5000
2020 [37]	In_2O_3	W (0.5 at%)	500	Spin-Coating	0.0054
2021 [38]	In_2O_3	Hf (0.5%M)	600	Spin-Coating	0.0400
2021 [39]	In_2O_3	Zr (1%M)	400	Spin-Coating	0.0730
2022 [40]	ZnO	-	160*	Spin-Coating	0.0217
This Work	In_2O_3	Zr (1%M)	400	Spin-Coating	0.672
This Work	In_2O_3	Zr (1%M)	400	Spin-Coating	2.822

Lastly, regarding the inkjet implementation, and considering the focus of this work, this step was approached as a "proof of concept", focusing in obtaining films and optimizing the uniformity of the films, rather than optimizing their electrical properties. The main variables studied were the UV substrate pre-treatment, which was fundamental for the solution adherence, resolution of the printing, in dots per inch (DPIs), that control the spacing between the drops and the overall usage of ink in a film. Lastly, the number of layers, in this case and as established before, was employed as a proof of concept that layers could be stacked. The results yielded from this last step showed that 15-minute UV pre-treatment at 4 cm distance from the lamp is enough for deposition and that the best resolution for printing with this solution is between 600 DPIs and 800 DPIs. As for the multiple layers study, it was inconclusive. Despite the inadequacy of the deposition, with poor adhesion of the second layer for the multiple DPIs studied, further investigation can lead to better results.

Upon the conclusion of this research, there are a few research-worthy parameters and studies to complement my own:

- Perform a study on the effects of relative humidity on TCO films properties.
- Continue the layer study by varying UV exposure, annealing temperature, and time between layers.
- Study the electrical properties of the printed films complemented with a thickness assessment.
- Further investigate inkjet printing, regarding different parameters such as UV exposure during deposition
- Employ the most promising film in devices requiring TCOs.

References

[1] M. Intelligence, “TRANSPARENT CONDUCTIVE FILMS MARKET - GROWTH, TRENDS, COVID-19 IMPACT, AND FORECASTS (2023 - 2028).” [Online]. Available: https://www.mordorintelligence.com/industry-reports/transparent-conductive-films-market. [Accessed: 20-Mar-2023].

[2] K. Research, “Global Transparent Conductive Films Market Size, Share & Industry Trends Analysis Report By Material, By Application (Smartphones, Notebooks, Tablets, Personal Computer, Wearables, and Others), By Regional Outlook and Forecast, 2022 - 2028.” [Online]. Available: https://www.kbvresearch.com/transparent-conductive-films-market/. [Accessed: 20-Mar-2023].

[3] Cognitive Market Research, “TCO Glass Market Report 2023 (Global Edition),” 2023. [Online]. Available: https://www.cognitivemarketresearch.com/tco-glass-market-report. [Accessed: 20-Mar-2023].

[4] R. M. Pasquarelli, D. S. Ginley, and R. O’hayre, “Solution processing of transparent conductors: From flask to film,” *Chem. Soc. Rev.*, vol. 40, no. 11, pp. 5406–5441, 2011, doi: 10.1039/c1cs15065k.

[5] R. A. Afre, N. Sharma, M. Sharon, and M. Sharon, “Transparent conducting oxide films for various applications: A review,” *Rev. Adv. Mater. Sci.*, vol. 53, no. 1, pp. 79–89, 2018, doi: 10.1515/rams-2018-0006.

[6] A. Stadler, “Transparent Conducting Oxides—An Up-To-Date Overview,” pp. 661–683, 2012, doi: 10.3390/ma5040661.

[7] New Atlas, “Touchscreen tech swaps rare metal for graphene, with no performance drop,” 2022. [Online]. Available: https://newatlas.com/electronics/indium-graphene-oled-touchscreen/. [Accessed: 10-Mar-2023].

[8] Lightinus, “SOLAR PANELS: HOW DO THEY WORK AND FUNCTION?,” 2017. [Online]. Available: https://www.lightinus.com/solar-panels-how-do-they-work-and-function/. [Accessed: 10-Mar-2023].

[9] Sun Vision Display, “How do Liquid Crystal Displays (LCDs) Work?,” 2020. [Online]. Available: https://www.sunvisiondisplay.com/how-do-lcds-work. [Accessed: 10-Mar-2023].

[10] Alliance7, “ELECTROCHROMIC (SMART GLASS),” 2018. [Online]. Available: https://www.alliance7.ca/blog/2018/7/18/electrochromic-smart-glass-view. [Accessed: 10-Mar-2023].

[11] K. Bädeker, “Über eine eigentümliche Form elektrischen Leitvermögens bei festen Körpern.” [Online]. Available: https://onlinelibrary.wiley.com/doi/10.1002/andp.19093340807?__cf_chl_jschl_tk__=pmd_QCVHmwh.4comN2kYrEcMvijC5SUVxuaYD1Oo.kpSNPg-1635261613-0-

gqNtZGzNAjujcnBszQlR. [Accessed: 26-Oct-2021].

[12] S. Sharma, S. Shriwastava, S. Kumar, K. Bhatt, and C. C. Tripathi, “Alternative transparent conducting electrode materials for flexible optoelectronic devices,” *Opto-electronics Rev.*, vol. 26, no. 3, pp. 223–235, 2018, doi: 10.1016/j.opelre.2018.06.004.

[13] M. Grundmann, “Karl Badeker (1877–1914) and the discovery of transparent conductive materials,” vol. 1426, no. 7, pp. 1409–1426, 2015, doi: 10.1002/pssa.201431921.

[14] T. O. L. Sunde *et al.*, “Transparent and conducting ITO thin films by spin coating of an aqueous precursor solution,” *J. Mater. Chem.*, vol. 22, no. 31, pp. 15740–15749, 2012, doi: 10.1039/c2jm32000b.

[15] M. Intelligence, “TRANSPARENT CONDUCTIVE FILMS MARKET - GROWTH, TRENDS, COVID-19 IMPACT, AND FORECASTS (2021 - 2026),” 2020. [Online]. Available: https://www.mordorintelligence.com/industry-reports/transparent-conductive-films-market. [Accessed: 26-Oct-2021].

[16] M. Intellica, “Global TCO Glass Market Research (2015-2019) and Future Forecast (2020-2025),” 2019. [Online]. Available: https://www.marketintellica.com/report/MI13777-global-tco-glass-market-research-2015. [Accessed: 26-Oct-2021].

[17] D. Li, W. Y. Lai, Y. Z. Zhang, and W. Huang, “Printable Transparent Conductive Films for Flexible Electronics,” *Adv. Mater.*, vol. 30, no. 10, pp. 1–24, 2018, doi: 10.1002/adma.201704738.

[18] Z. Chen, W. Li, R. Li, Y. Zhang, G. Xu, and H. Cheng, “Fabrication of highly transparent and conductive indium-tin oxide thin films with a high figure of merit via solution processing,” *Langmuir*, vol. 29, no. 45, pp. 13836–13842, 2013, doi: 10.1021/la4033282.

[19] A. C. Dippel, T. Schneller, P. Gerber, and R. Waser, “Morphology control of highly-transparent indium tin oxide thin films prepared by a chlorine-reduced metallo-organic decomposition technique,” *Thin Solid Films*, vol. 515, no. 7–8, pp. 3797–3801, 2007, doi: 10.1016/j.tsf.2006.09.045.

[20] Y. C. Liang and Y. C. Liang, “Physical properties of low temperature sputtering-deposited zirconium-doped indium oxide films at various oxygen partial pressures,” *Appl. Phys. A Mater. Sci. Process.*, vol. 97, no. 1, pp. 249–255, 2009, doi: 10.1007/s00339-009-5214-2.

[21] C. I. Bright, *Chapter 21 - Transparent conductive thin films*. Elsevier LTD., 2018.

[22] F. Ruske, “Deposition and Properties of TCOs,” pp. 301–330, 2012.

[23] A. Facchetti and T. Marks, *Transparent Electronics: From Synthesis to Applications*, First. Wiley, 2010.

[24] J. Xu, J. B. Liu, B. X. Liu, S. N. Li, S. H. Wei, and B. Huang, “Design of n-Type Transparent Conducting Oxides: The Case of Transition Metal Doping in In2O3,” *Adv. Electron. Mater.*, vol. 4, no. 3, pp. 1–7, 2018, doi: 10.1002/aelm.201700553.

[25] R. Branquinho *et al.*, “Solution Combustion Synthesis: Applications in Oxide Electronics,” *Intech*, vol. i, no. tourism, p. 13, 2016.

[26] A. Renhuai Wei, a Xianwu Tang, a Ling Hu, a Jie Yang, a Xiaoguang Zhu, a Wenhai Song, a Jianming Dai and a and Y. S. Xuebin Zhu, “Facile Chemical Solution Synthesis in an Open Condition for p- Type Delafossite Ag-based Transparent Conducting AgCrO2 Films,” *J. Mater. Chem. C*, 2017, doi: 10.1039/C6TC04848J.

[27] F. Hermerschmidt, S. A. Choulis, and E. J. W. List-Kratochvil, “Implementing Inkjet-Printed Transparent Conductive Electrodes in Solution-Processed Organic Electronics,” *Adv. Mater. Technol.*, vol. 4, no. 5, pp. 1–16, 2019, doi: 10.1002/admt.201800474.

[28] B. M. Singh, H. M. Haverinen, P. Dhagat, and G. E. Jabbour, “Inkjet Printing — Process and Its Applications,” vol. 90014, pp. 673–685, 2010, doi: 10.1002/adma.200901141.

[29] S. Seki *et al.*, “Highly conducting indium-tin-oxide transparent films prepared by dip-coating with an indium carboxylate salt,” vol. 170, pp. 525–527, 2003, doi: 10.1016/S0257-8972(03)00170-1.

[30] D. Spiehl, M. Häming, H. M. Sauer, K. Bonrad, and E. Dörsam, “Engineering of Flexo- and Gravure-Printed Indium – Zinc-Oxide Semiconductor Layers for High-Performance Thin-Film Transistors,” vol. 62, no. 9, pp. 2871–2877, 2015, doi: 10.1109/TED.2015.2449665.

[31] E. Carlos, R. Branquinho, P. Barquinha, R. Martins, and E. Fortunato, *New strategies toward highperformance and low-temperature processing of solution-based metal oxide TFTs*. 2021.

[32] E. Carlos, R. Martins, E. Fortunato, and R. Branquinho, “Solution Combustion Synthesis: Towards a Sustainable Approach for Metal Oxides,” *Chem. - A Eur. J.*, vol. 26, no. 42, pp. 9099–9125, 2020, doi: 10.1002/chem.202000678.

[33] F. Deganello and A. Kumar, “Solution combustion synthesis , energy and environment : Best parameters for better materials,” *Prog. Cryst. Growth Charact. Mater.*, vol. 64, no. 2, pp. 23–61, 2018, doi: 10.1016/j.pcrysgrow.2018.03.001.

[34] O. Malik, F. Javier, and D. Hidalga, “Sputtered Indium Tin Oxide Films for Optoelectronic Applications.”

[35] B. H. Kim *et al.*, “High Mobility in Nanocrystal-Based Transparent Conducting Oxide Thin Films,” 2018, doi: 10.1021/acsnano.7b06783.

[36] P. Pujar, R. V. Vardhan, D. Gupta, and S. Mandal, “A balancing between super transparency and conductivity of solution combustion derived titanium doped indium oxide: Effect of charge carrier density and mobility,” *Thin Solid Films*, vol. 660, no. June, pp. 267–275, 2018, doi: 10.1016/j.tsf.2018.06.031.

[37] Y. Liu *et al.*, “Solution processed W-doped In2O3 thin films with high carrier mobility,” *Ceram. Int.*, vol. 46, no. 2, pp. 2173–2177, 2020, doi: 10.1016/j.ceramint.2019.09.201.

[38] R. Firmino *et al.*, “Solution Combustion Synthesis of Hafnium-Doped Indium Oxide Thin Films for Transparent Conductors,” 2022, doi: 10.3390/nano12132167.

[39] R. Maria and G. Firmino, “MATERIALS SCIENCE BSc in Materials Engineering Sciences SOLUTION PROCESSING OF DOPED INDIUM OXIDE FOR APPLICATIONS AS TRANSPARENT CONDUCTING OXIDES,” 2021.

[40] Z. Chen *et al.*, “A Transparent Electrode Based on Solution- Processed ZnO for Organic Optoelectronic Devices,” pp. 1–12, 2022, doi: 10.1038/s41467-022-32010-y.

[41] D. Corzo *et al.*, “Digital Inkjet Printing of High-Efficiency Large-Area Nonfullerene Organic Solar Cells,” vol. 1900040, pp. 1–9, 2019, doi: 10.1002/admt.201900040.

[42] J. Jeong, J. Kim, and H. Kim, “Solar Energy Materials & Solar Cells Ag grid / ITO hybrid transparent electrodes prepared by inkjet printing,” *Sol. Energy Mater. Sol. Cells*, vol. 95, no. 7, pp. 1974–1978, 2011, doi: 10.1016/j.solmat.2011.02.016.

[43] Z. Zhan, J. An, Y. Wei, V. Thai Tran, and H. Du, “Inkjet-printed optoelectronics,” *Nanoscale*, 2016, doi: 10.1039/C6NR08220C.

[44] L. Nayak, S. Mohanty, S. K. Nayak, and A. Ramadoss, “A review on inkjet printing of nanoparticle inks for flexible electronics,” *J. Mater. Chem. C*, vol. 7, no. 29, pp. 8771–8795, 2019, doi: 10.1039/c9tc01630a.

[45] Merck, “IR Spectrum Table & Chart.” [Online]. Available:

https://www.sigmaaldrich.com/PT/en/technical-documents/technical-article/analytical-chemistry/photometry-and-reflectometry/ir-spectrum-table. [Accessed: 03-Jul-2022].

[46] M. Manivannan, S. Rajendran, and A. A. Nagar, “INVESTIGATION OF INHIBITIVE ACTION OF UREA- ZN 2 + SYSTEM IN THE CORROSION CONTROL OF,” no. November 2011, 2015.

[47] “Viscosity Table Print.” [Online]. Available: https://www.accudynetest.com/visc_table_print.html?sortby=sort_molecular_weight. [Accessed: 02-Oct-2022].

[48] A. Paula, S. Capuci, N. D. De Carvalho, M. R. F. Jr, and R. A. Malagoni, “Solubility of Urea in ethanol-water mixtures and Solubilidad de Urea en mezclas de etanol-agua y etanol puro a temperaturas de 278 , 1K a 333 , 1K Solubilidade da Ureia em misturas de etanol-água e em etanol puro em temperaturas de 278 , 1K a 333 , 1K,” vol. 29, no. 2, pp. 125–133, 2016.

[49] F. Lee and L. E. Lahti, “Solubility of Urea in Water-Alcohol Mixtures,” vol. 17, no. 3, pp. 304–306, 1972.

[50] C. Guillén and J. Herrero, “Critical review TCO / metal / TCO structures for energy and fl exible electronics,” *Thin Solid Films*, vol. 520, no. 1, pp. 1–17, 2011, doi: 10.1016/j.tsf.2011.06.091.

[51] Chemical Book, “Ethylene glycol.” [Online]. Available: https://www.chemicalbook.com/ChemicalProductProperty_EN_CB7852707.htm. [Accessed: 02-Oct-2022].

[52] ChemSpider, “Methoxyethanol.” [Online]. Available: http://www.chemspider.com/Chemical-Structure.7728.html. [Accessed: 02-Oct-2022].

[53] “Spin Coating: Complete Guide to Theory and Techniques.” [Online]. Available: https://www.ossila.com/en-eu/pages/spin-coating. [Accessed: 20-Nov-2022].

[54] B. Parija and S. Panigrahi, “Fundamental understanding and modeling of spin coating process : A review,” vol. 83, pp. 493–502, 2009, doi: 10.1007/s12648-009-0009-z.

[55] C. J. Lawrence, “The mechanics of spin coating of polymer films,” *Phys. Fluids*, vol. 31, no. 10, pp. 2786–2795, 1988, doi: 10.1063/1.866986.

[56] P. Yu *et al.*, “Microstructure and local electrophysical properties of sol-gel derived (In 2 O 3 - 10 % SnO 2)/ V 2 O 5 films,” *Colloid Interface Sci. Commun.*, vol. 43, no. June, p. 100452, 2021, doi: 10.1016/j.colcom.2021.100452.

[57] Accu Dyne Test, “Surface tension values of some common test liquids for surface energy analysis.” [Online]. Available: http://www.surface-tension.de. [Accessed: 29-Nov-2022].

[58] PubChem, “2-Methoxyethanol (Compound).” [Online]. Available: https://pubchem.ncbi.nlm.nih.gov/compound/2-Methoxyethanol#section=Heat-of-Vaporization. [Accessed: 20-Nov-2022].

[59] PubChem, “Ethanol (Compound).” [Online]. Available: https://pubchem.ncbi.nlm.nih.gov/compound/702#section=Heat-of-Vaporization. [Accessed: 20-Nov-2022].

[60] PubChem, “Ethylene Glycol (Compound).” [Online]. Available: https://pubchem.ncbi.nlm.nih.gov/compound/174#section=Heat-of-Vaporization. [Accessed: 20-Nov-2022].

A.

FTIR of the Precursors

FTIR spectra for the different solvents and precursors are presented in:

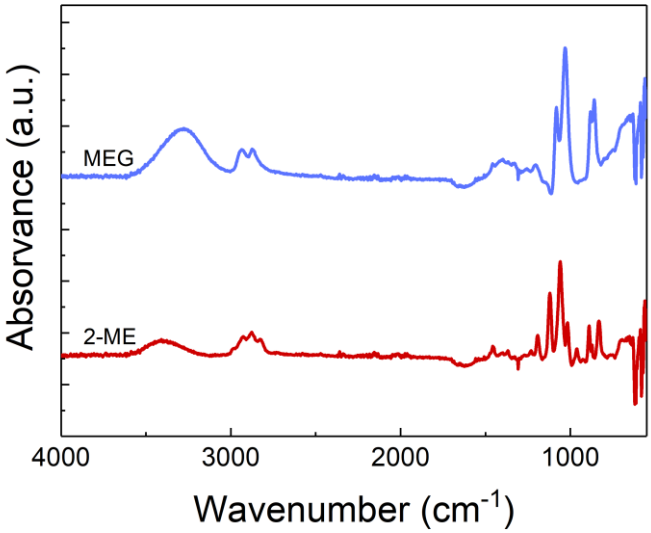

Figure A.1- FTIR spectra for EG and 2-ME reactants.

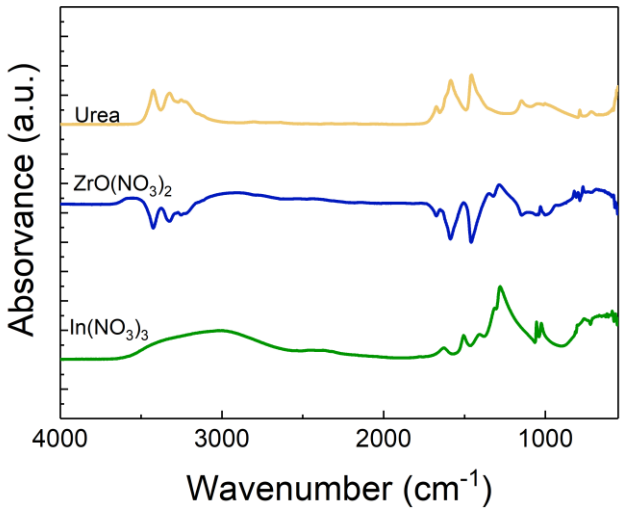

Figure A.2- FTIR spectra for urea, indium and Zr precursors.

B.

Z-Value calculation

To better compare the inkjet printing potential between the different solutions the z-value had to be calculated. The z-value is defined as the inverse Ohnesorge number and compiles the different relevant parameters in order to assess the printability of a certain ink. The equation defining the Z-Value is as presented:

$$Z = Oh^{-1} = \frac{\sqrt{\rho\gamma d}}{\eta} \tag{B.1}$$

Where ρ is the density, γ the surface tension, d the nozzle size and η the dynamic viscosity of the fluid.

For this work, the nozzle used had 21 µm of diameter, the viscosity values used for the calculation were taken from the measures taken and the values used for the surface tension and density of the different components of the ink solution are presented in the following table:

Table B.1- Physical properties at 25°C of the different solvents used for the calculations of the Z-value.

Solvent	Density (g/cm^3)	Surface Tension (mN/m)
2-ME	0.96 [57]	30.84[58]
Ethanol	0.79 [57]	22.10[59]
Water	1.00 [57]	72.70[57]
EG	1.11 [57]	47.70[60]

C.
Ellipsometry Fitting and Results

All ellipsometry measurements, except for the film from 2ME solution with 0% (V/V) EG, present the fitting bellow. Allowing an analysis of the adequacy of the measurement.

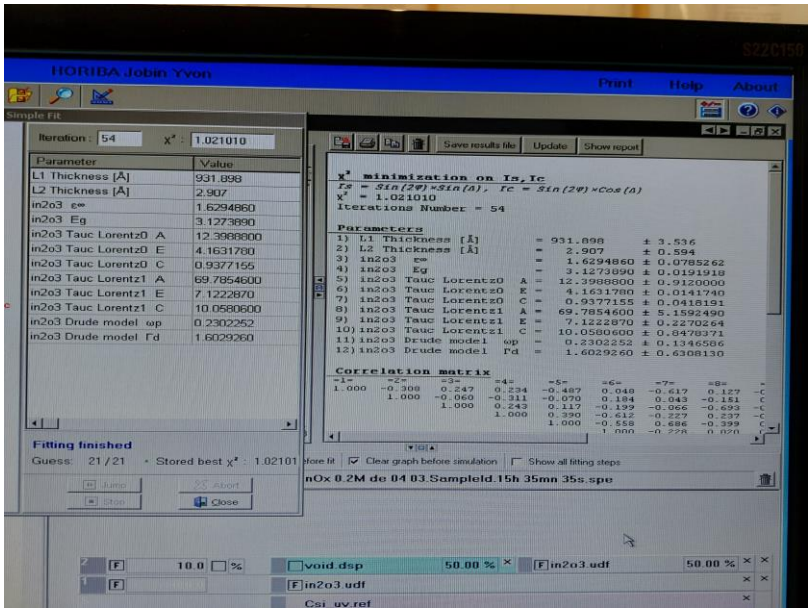

Figure C.1 - 2-ME 0%(V/V) EG ellipsometry measurements

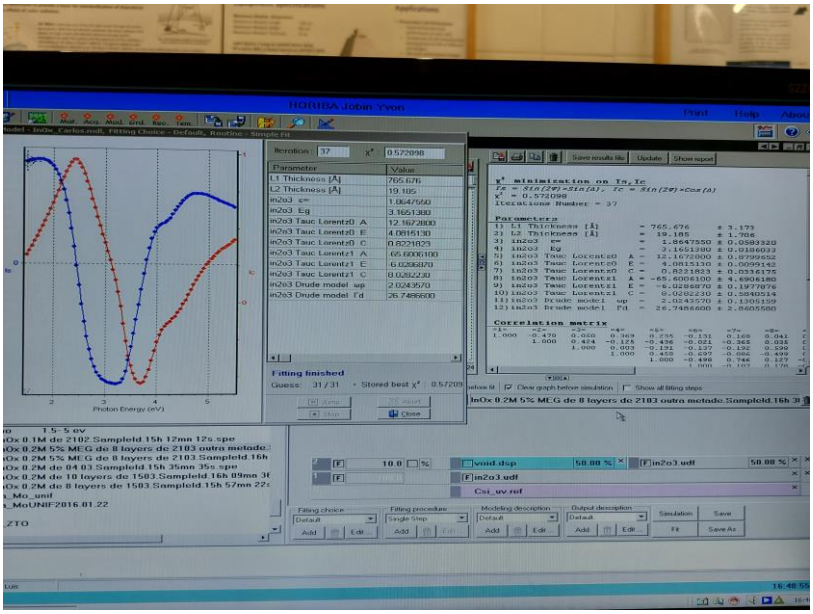

Figure C.2 - 2-ME 5%(V/V) EG ellipsometry measurements

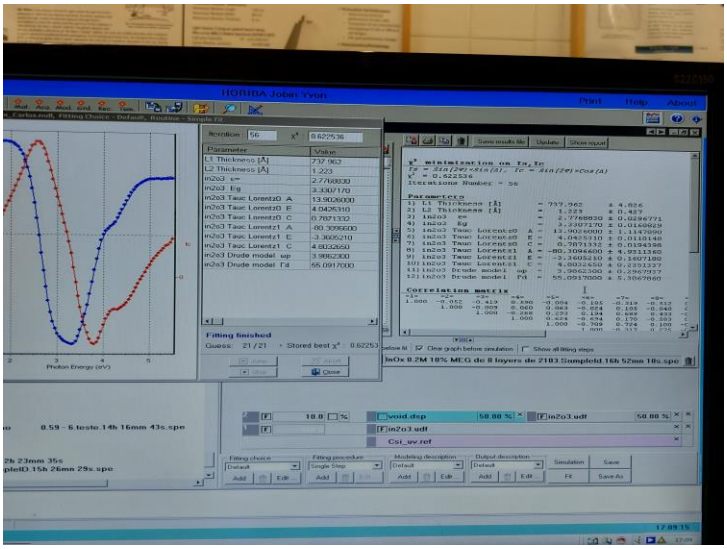

Figure C.3 - 2-ME 10%(V/V) EG ellipsometry measurements

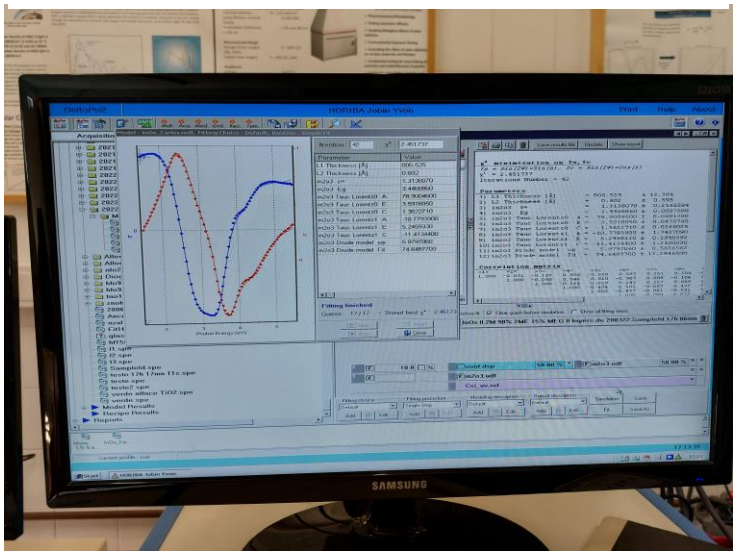

Figure C.4 - 2-ME 15%(V/V) EG ellipsometry measurements

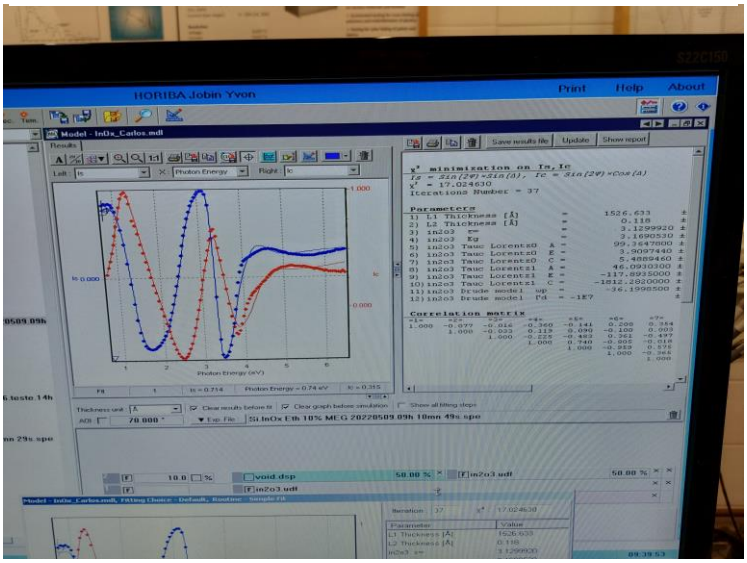

Figure C.3- ETH 10%(V/V) EG ellipsometry measurements

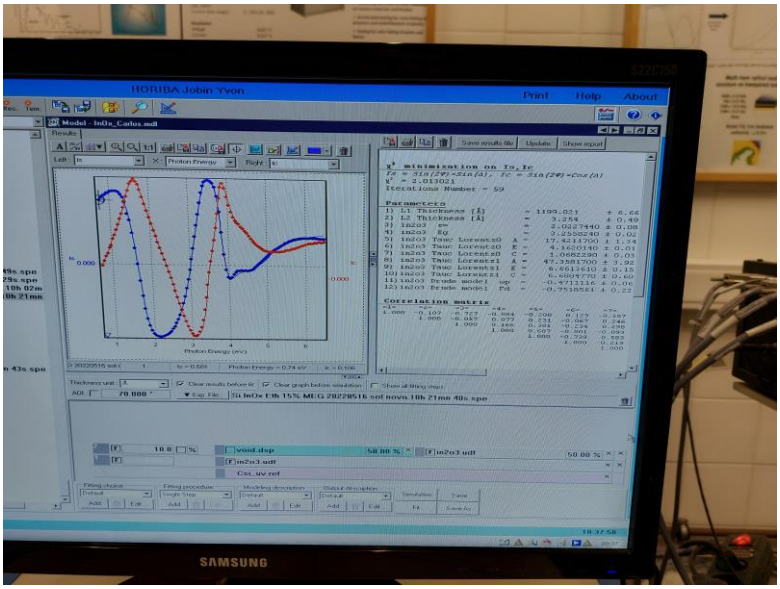

Figure C.6 - ETH 15%(V/V) EG ellipsometry measurements

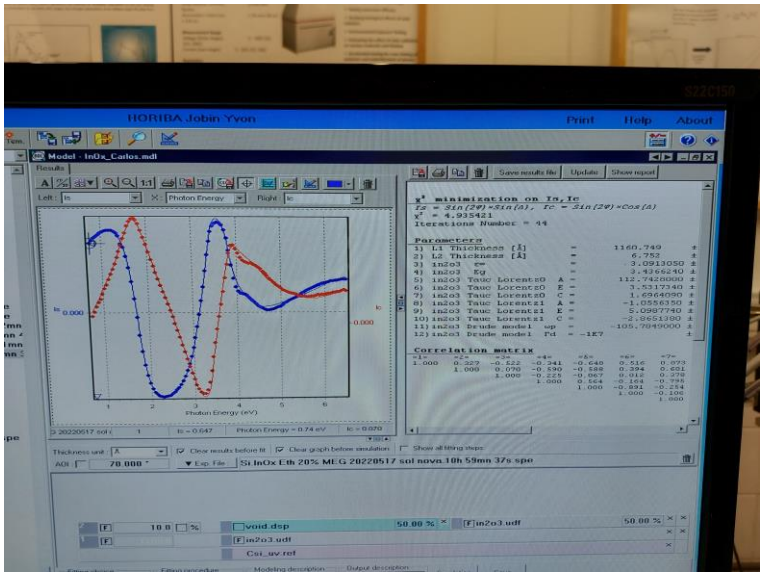

Figure C.7 - ETH 20%(V/V) EG ellipsometry measurements

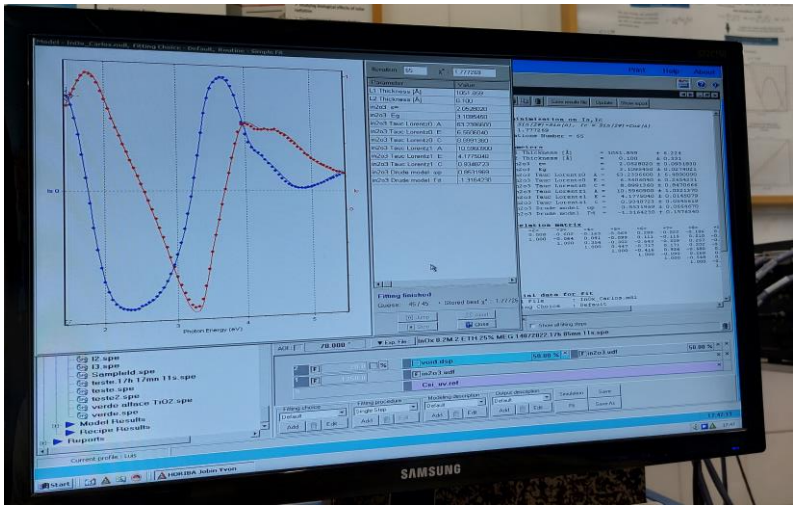

Figure C.8 - ETH 25%(V/V) EG ellipsometry measurements

D.

Chemical characterization of films with different number of layers

The FTIR analysis provides valuable information regarding the chemical composition of the sample. Following the relevant results presented, the FTIR analysis for the 2-ME 0.2M Zr-doped In_2O_3 thin films.

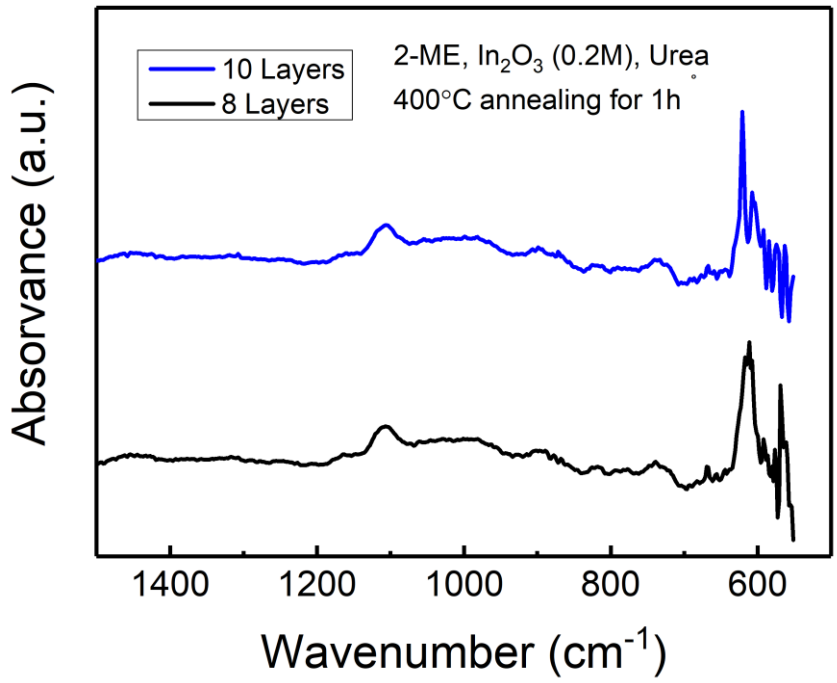

Figure D.1 - FTIR spectra for 2-ME based films, with In2O3 concentration of 0.2M and a 1h annealing at 400°C for both 8 and 10 layers thin films

Considering the solution used is the same so is the deposition process, no difference is noted, as expected.

E.

Chemical characterization of EG influence on thin films

In order to control the viscosity of the solution EG was added and the following FTIR spectra presents the chemical differences this addition brings to the chemical composition of the thin films.

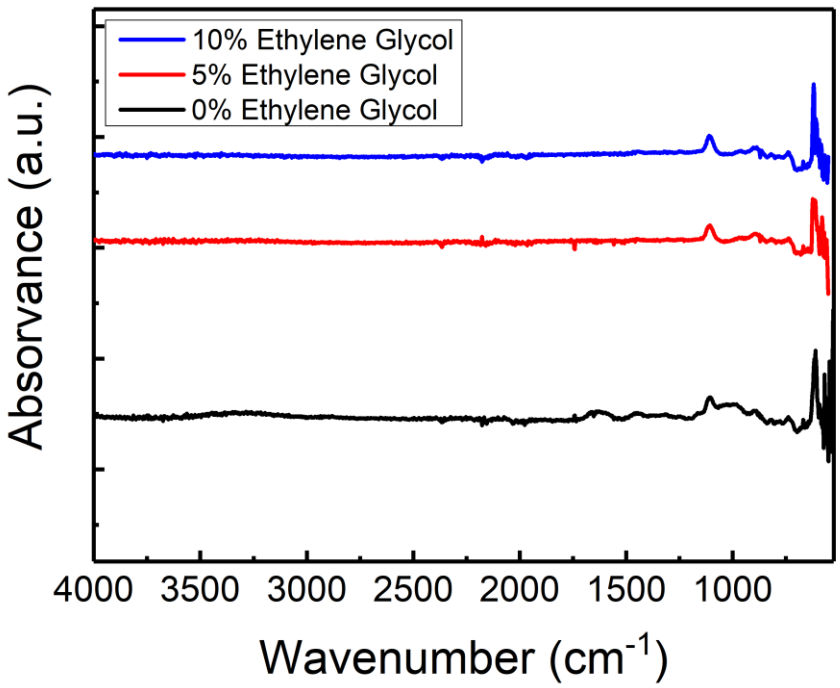

Figure E.1- FTIR spectra for 8-layer InOx thin films based in 2-ME solutions with EG concentrations from 0% to 10%

Despite the addition, no relevant influence was noted in chemical composition.

F.

Bandgap Calculation

The bandgap is an important property for any TCO as it relates with the transparency of said TCO. In order to accomplish transparency, the bandgap ought to be superior to 3 eV, to allow visible light part of the spectrum to pass through the material. The bandgap E_{opt} was calculated by firstly determining the absorption coefficient (α) following the equation:

$$\alpha = \frac{1}{d_s}\ln\left(\frac{1-R}{T}\right) \quad \text{(E.1)}$$

where d_s is the film thickness, R the reflectance and T the transmittance. Both the reflectance and the transmittance UV-Vis spectra follow:

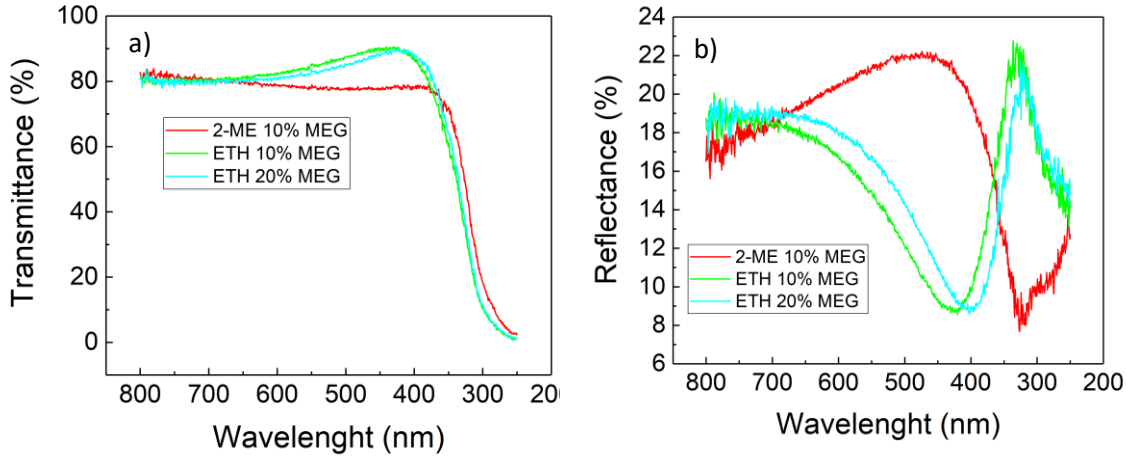

Figure F.1 - a) Transmittance and b) Reflectance spectra for different thin films

Once the absorption coefficient was calculated, the Tauc equation:

$$\alpha h\nu = A(h\nu - E_{opt})^n \quad \text{(E.2)}$$

where ν is the frequency of the incident radiation, h the Planck's constant can be employed to determine the bandgap. A is a constant and n a value that depends on the type of optical transition which in this case assumes the value of 1/2 given direct transitions are allowed. Lastly the optical bandgap values are obtained by plotting $(\alpha h\nu)^2$as a function of $h\nu$ and extrapolating the linear region to find the intersection $(\alpha h\nu)^2 = 0$. The resulting plots are presented in figure 3.14.

G.

Complete topography measured by profilometry

The complete topography of the printed squares for different resolutions.

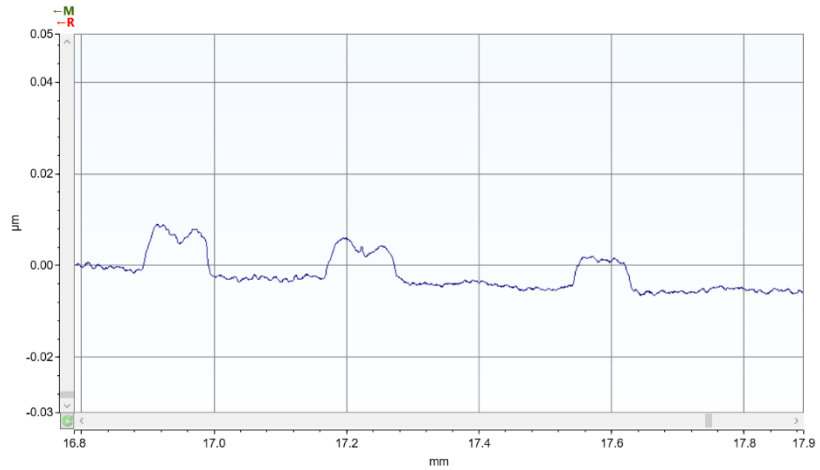

Figure G.1 - Topography for 100 DPI, Zr-doped In2O3 printed film

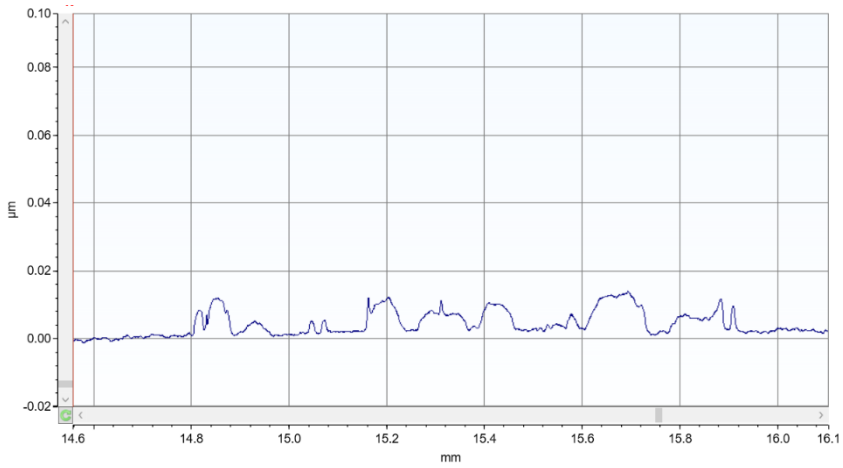

Figure G.2 - Topography for 200 DPI, Zr-doped In2O3 printed film

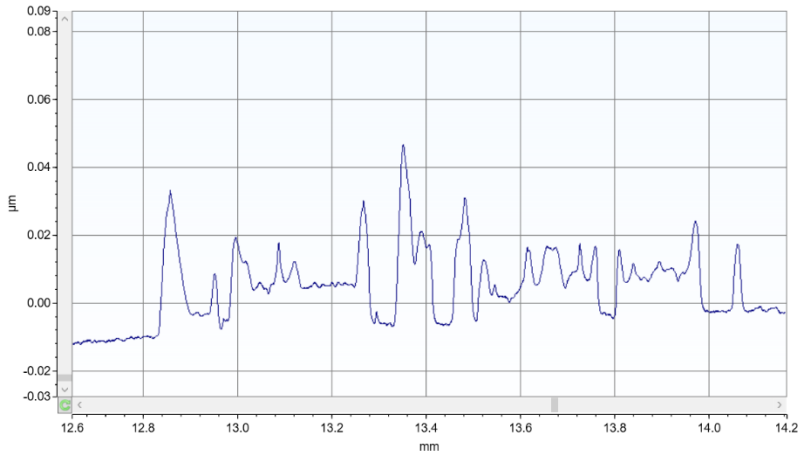

Figure G.3 - Topography for 400 DPI, Zr-doped In2O3 printed film

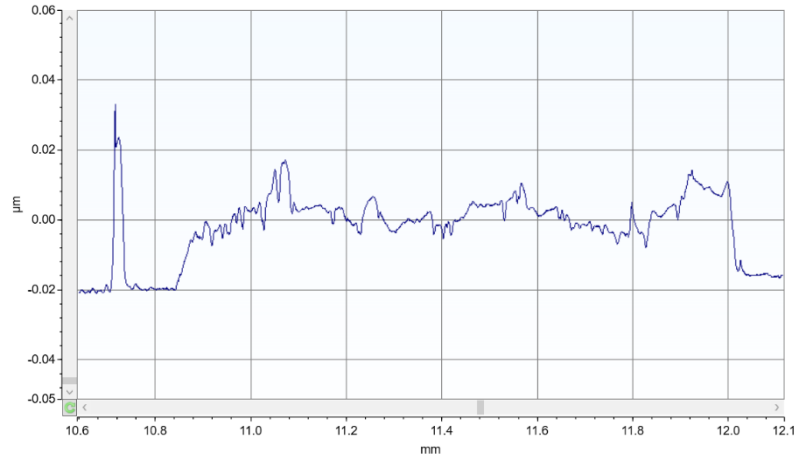

Figure G.4 - Topography for 600 DPI, Zr-doped In2O3 printed film

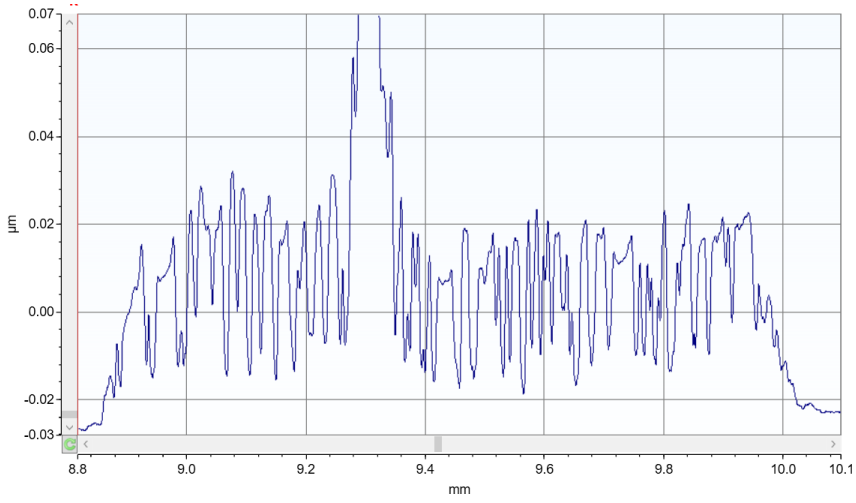

Figure G.5 - Topography for 800 DPI, Zr-doped In2O3 printed film

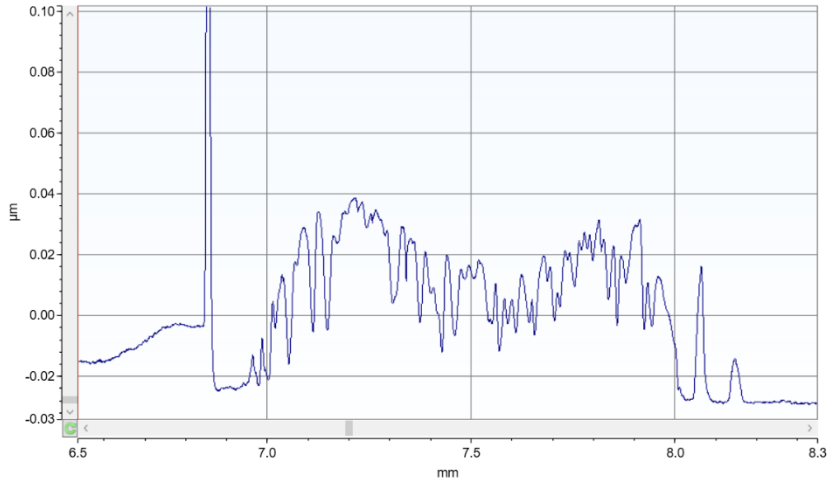

Figure G.6 - Topography for 1000 DPI, Zr-doped In2O3 printed film

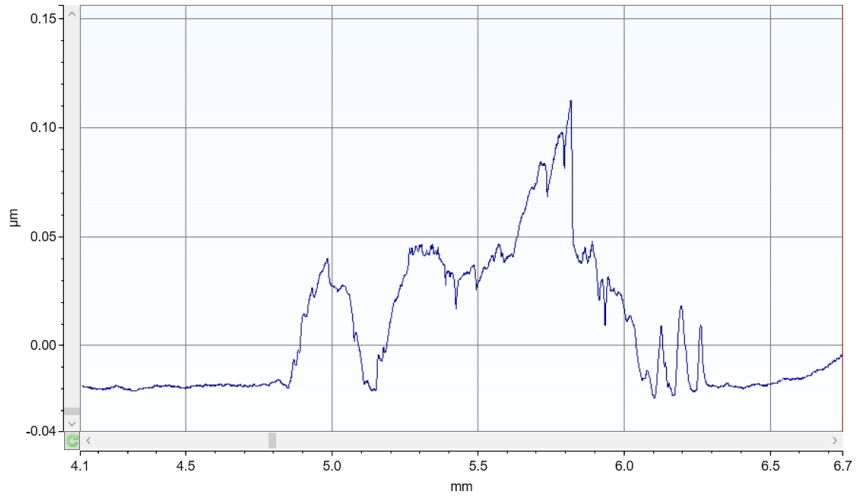

Figure G.7 - Topography for 1200 DPI, Zr-doped In2O3 printed film

2023

TOMÁS FRANCISCO PRIOR VICENTE DE MEDEIROS PEREIRA

PRINTED TRANSPARENT CONDUCTIVE OXIDES FOR ELECTRONIC APPLICATIONS

NOVA SCHOOL OF SCIENCE & TECHNOLOGY